Covarrubias Alejandra A (Orcid ID: 0000-0003-0439-3414)
Reyes José Luis (Orcid ID: 0000-0001-5129-9741)

N6-Methyladenosine modification of mRNA contributes to the transition from 2D to 3D growth in the moss *Physcomitrium patens*

David Garcias-Morales[1], V. Miguel Palomar[2], Florence Charlot[3], Fabien Nogué[3], Alejandra A. Covarrubias[1], José L. Reyes[1]

[1]Departamento de Biología Molecular de Plantas, Instituto de Biotecnología, UNAM. Av. Universidad 2001, CP 62210, Cuernavaca, Mor. MEXICO.
[2]Department of Molecular, Cellular and Developmental Biology, University of Michigan, 1105 N. University Ave. Ann Arbor, MI 48109-1085, USA.
[3]Université Paris-Saclay, INRAE, AgroParisTech, Institut Jean-Pierre Bourgin (IJPB), 78000, Versailles, France.

Corresponding Author
José L. Reyes
Departamento de Biología Molecular de Plantas, Instituto de Biotecnología, UNAM. Av. Universidad 2001, CP 62210, Cuernavaca, Mor. MEXICO. jose.reyes@ibt.unam.mx

Keywords: MTA, MTB, FIP37, PpAPB, epitranscriptome, gametophore bud formation.

This is the author manuscript accepted for publication and has undergone full peer review but has not been through the copyediting, typesetting, pagination and proofreading process, which may lead to differences between this version and the Version of Record. Please cite this article as doi: 10.1111/tpj.16149

ABSTRACT

Plants colonized the land ca. 470 million years ago, coinciding with the development of apical cells that divide in three planes. The molecular mechanisms that underly the regulation of the 3D growth pattern are poorly understood, mainly because 3D growth in seed plants starts during embryo development. In contrast, the transition from 2D to 3D growth in the moss *Physcomitrium patens* has been widely studied and it involves a large turnover of the transcriptome to allow the establishment of stage-specific transcripts that facilitate this developmental transition. N6-methyladenosine (m^6A) is the most abundant, dynamic, and conserved internal nucleotide modification present on eukaryotic mRNA and serves as a layer of post-transcriptional regulation directly affecting several cellular processes and developmental pathways in many organisms. In Arabidopsis, m^6A has been reported to be essential for organ growth and determination, embryo development and responses to environmental signals. In this study, we identified the main genes of the m^6A methyltransferase complex (MTC) *MTA*, *MTB* and *FIP37*, in *P. patens* and demonstrate that their inactivation leads to loss of m^6A in mRNA, a delay in the formation of gametophore buds, and defects in spore development. Genome-wide analysis revealed several transcripts affected in the *Ppmta* background. We demonstrate that the *PpAPB1-4* transcripts, encoding for central factors regulating the 2D to 3D transition in *P. patens*, are m^6A-modified, while in the *Ppmta* mutant the lack of the m^6A mark is associated with a corresponding decrease in transcript accumulation. Overall, we suggest that m^6A is essential to enable the proper accumulation of these and other bud-specific transcripts directing the turnover of stage-specific transcriptomes, and thus promoting the transition from protonema to gametophore buds in *P. patens*.

INTRODUCTION

One of the main characteristics that allowed plants to colonize the land 470 million years ago was the development of apical cells that divide in three planes (Graham *et al.*, 2000). Apical cells are present in the lineage of charophycean algae from which land plants originated, nevertheless these organisms grow only in either one or two planes, therefore, creating a net of filaments or branching mats (Niklas, 2000). Later in evolution, plant apical cells gained the ability to divide in three dimensions (3D), allowing the acquisition of a new array of shapes and the colonization of new spaces.

The molecular mechanisms that underly the regulation of 3D growth are poorly understood, mainly because 3D growth in seed plants starts during embryo development, and therefore, mutants exhibiting defects in 3D growth are lethal (Meinke and Sussex, 1979; Sun *et al.*, 1998). The life cycle of the moss *Physcomitrium patens* recapitulates the transition from filamentous growth to planar branching, to full 3D growth and a similar transition occurs later during the development of its zygote (Cove and Knight, 1993; Govindan *et al.*, 2022; Harrison *et al.*, 2009). Nonetheless, mutations in genes involved in the transition from 2D to 3D growth are not lethal as plants can survive by filamentous growth indefinitely (Moody *et al.*, 2018), turning *P. patens* into an ideal model to study 3D growth regulation in plants.

The life cycle of *P. patens* starts with the germination of a haploid spore from which a filamentous structure called protonema emerges, growing by uniplanar cell division; the protonema is composed of two cell types, chloronema which has numerous chloroplasts and caulonema which contains oblique cell walls and fewer chloroplasts (Cove *et al.*, 2006; Menand *et al.*, 2007). The 2D growth form continues when the subapical cells divide, originating side branches called secondary protonema, however, some of the subapical cells can divide in a new 3D growth pattern to give rise to stem cells named gametophore buds (Aoyama *et al.*, 2012; Cove and Knight, 1993; Harrison *et al.*, 2009). These buds divide in three planes to first develop into gametophores, which are composed of leaf-like structures known as phyllids and root-like rhizoids; gametophores later develop sexual organs: female archegonia and male antheridia. The diploid zygote is originated when the egg is fertilized by one flagellated sperm cell, this zygote undergoes 3D growth to generate the sporophyte composed of foot, seta, and capsule where thousands of haploid spores are produced by meiosis to complete the life cycle (Harrison *et al.*, 2009).

The transition from 2D to 3D growth in *P. patens* has been widely studied and a mechanism for its regulation has been proposed (Moody, 2019). The principal regulators of this transition are the PpAPB transcription factors, which are the orthologs of the Arabidopsis AINTEGUMENTA, PLETHORA, and BABY BOOM proteins. These transcription factors (PpAPB1 to 4) are indispensable for the formation of gametophore buds and a quadruple mutant is incapable of forming gametophore initial cells (Aoyama *et al.*, 2012). Transcription of the *PpAPB* genes is affected in the absence of DEFECTIVE KERNEL 1 (PpDEK1) (Demko *et al.*, 2014; Johansen *et al.*, 2016; Perroud *et al.*, 2014) and NO GAMETOPHORES 1 (PpNOG1)(Moody *et*

al., 2018). Thus, the current proposed mechanism suggests that PpDEK1, a calpain protease, represses the transcription of the *PpAPB* genes by cleaving a putative transcription activator, whereas PpNOG1 would promote their transcription by targeting a putative repressor for ubiquitination and ensuing degradation (Moody *et al.*, 2018). More recent evidence has suggested that PpNOG1 could directly regulate the subcellular accumulation of DEK1, pointing to another path for *APB* regulation (Perroud *et al.*, 2020). The transcription of the *PpAPB* genes is also upregulated by auxins. Once the transcription of these genes is achieved, the transition from 2D to 3D is initiated, promoting the activation of several cytokinin response regulators (Aoyama *et al.*, 2012). However, other participants in this process remain to be discovered. In particular, the transition from 2D to 3D growth in *P. patens* has been shown to involve a large turnover of the transcriptome and this process has to be finely regulated to allow the establishment of a set of stage-specific transcripts that facilitate the transition to a 3D growth pattern (Frank and Scanlon, 2015).

There are numerous posttranscriptional mechanisms known to regulate mRNA abundance, among them, addition of N6-methyladenosine (m^6A), an mRNA chemical modification, has recently emerged as a process to directly control the metabolism of the transcripts at the transcriptome level (Frye *et al.*, 2018; Ivanova *et al.*, 2017; Wang *et al.*, 2021). m^6A is the most abundant and well characterized internal mRNA modification and its transcriptome landscape is dynamically regulated by the activity of different proteins which install (m^6A methyltransferases), remove (m^6A demethylases), and recognize (m^6A-binding factors) this modification (Shi *et al.*, 2019). The addition of the methyl group is catalyzed by a large methyltransferase complex (MTC) in which the METTL3/METTL14 (methyltransferase-like 3/14) heterodimer acts as the catalytic core, and WTAP (Wilms' tumor 1-associated protein) allows the interaction with several protein factors that modulate its activity (Garcias Morales and Reyes, 2021). In plants, the MTC has been identified and orthologs of METTL3, METTL14 and WTAP, named respectively, MTA, MTB and FIP37 have been studied, mostly in *Arabidopsis thaliana* (Bodi *et al.*, 2012; Růžička *et al.*, 2017; Shen *et al.*, 2016; Zhong *et al.*, 2008). The biological effects of m^6A modification of mRNA in plants are diverse, including regulation of organ growth and determination (Arribas-Hernández *et al.*, 2018; Růžička *et al.*, 2017; Shen *et al.*, 2016), embryo development (Zhong *et al.*, 2008) and responses to environmental signals (Anderson *et al.*, 2018; Govindan *et al.*, 2022; Hu *et al.*, 2021).

Here, we identified the gene orthologs of *MTA*, *MTB* and *FIP37* in the moss *P. patens* and demonstrate that the m^6A methyltransferase activity on mRNA is abolished in the null mutants of these genes. The absence of m^6A in mRNA leads to defects in the moss life cycle, as shown by a delay in gametophore bud formation and defects in spore development and viability. Unlike *A. thaliana*, the mutant plants of the MTC are viable and can be propagated indefinitely by protonemal growth. We demonstrate that transcripts of all four *PpAPBs* are methylated and that the absence of methylation in *Ppmta* mutant plants drives the decrease of these transcripts, resulting in a delay in the transition from 2D to 3D growth. We propose that m^6A modification of mRNA is required to facilitate the transition from 2D to 3D growth by regulating the abundance of several mRNAs, including the *PpAPB* transcripts, encoding for the master regulators of this developmental pathway.

METHODS

Cloning and purification of sgRNA plasmids

Coding sequences for the *PpMTA*, *PpFIP37*, *PpMTB1* and *PpMTB2* genes were used to search for CRISPR RNA (crRNA) preceded by a PAM motif of the *Streptococcus pyogenes* Cas9 (NGG or NAG) using the webtool CRISPOR V1 (http://crispor.tefor.net/crispor.py) and the *P. patens* genome V3 (https://phytozome-next.jgi.doe.gov/info/Ppatens_v3_3). We selected crRNAs near the translation start codon with a high specificity score.

Moss culture and Protoplast transformation

The Gransden wild-type strain of *P. patens* was used for this study. The moss was cultured on PpNH4 medium (Charlot *et al.*, 2022), propagated in Percival growth chambers (Geneva Scientific, Fontana, WI) set to 25 °C and 60 % humidity with a photoperiod of 16 h light/8 h dark under white light (80 μmol m^{-2} sec^{-1}). Protoplast isolation was performed following a previously described protocol (Charlot *et al.*, 2022). Protoplasts were incubated with 10 μg of pAct-Cas9 plasmid (Lopez-Obando *et al.*, 2016) containing the coding sequence for the protein Cas9 and with 10-12 μg of the sgRNA plasmid for the single mutants or a mix of 10-12 μg of sgRNA plasmids for the multiple mutants. The amount of each sgRNA plasmid in the mix was obtained by dividing the total amount of sgRNA plasmids (10–12 μg) by the number of sgRNA plasmids used for each transformation as described before (Lopez-Obando *et al.*, 2016). The protoplasts were regenerated on PpNH4 medium supplemented with 0.33 M mannitol for 1 week, then the plants on cellophane disks were transferred to PpNH4 medium supplemented with 50 μg/L of G418 for plasmid selection. The transfected plants were placed on a new PpNH4 plate without selection and after 1 week were isolated.

Genotyping using PCR screening

After 1 month of growth, individual plants were used for DNA extraction. The tissue was frozen in liquid nitrogen and ground to a fine powder. DNA extraction was performed using 2X CTAB buffer (2 % acetyl-trimethylammonium bromide, 1 % polyvinyl pyrrolidone, 100 mM Tris-HCl, pH 8.0, 1.4 M NaCl, 20 mM EDTA). For each sample, 500 µl of 2x CTAB Extraction Buffer were used, samples were mixed and transferred to a 60 °C thermoblock for 30 min, then the samples were centrifuged at 14,000 x g for 5 min; the supernatant was transferred to a new tube, an equal volume of chloroform was added, mixed and after 5 min of centrifugation at 14,000 x g the phases were separated. The aqueous upper phase was transferred to a new tube and the DNA was precipitated by adding 0.7 volumes of cold isopropanol and centrifuged at 14,000 x g for 10 min. The supernatant was discarded, and precipitated DNA was rinsed by adding 500 µl of 75 % ethanol, and centrifuged for 5 min at 14,000 x g. The recovered genomic DNA was dissolved in 50 µl of water. To identify CRISPR/Cas9-generated mutations, the primers used for the PCR were designed to surround

the target sequence and to amplify 150-200 bp fragments (Table S1). The PCR reactions (50 µl) were performed using 1 µl of DNA sample as template. The resulting DNA fragments were evaluated by 3 % agarose TAE gel-electrophoresis and when a change in size was observed, the fragment was sequenced (Unidad de Síntesis y Secuenciación de DNA, IBt UNAM, Mexico).

Generation of complemented lines

A 2000 bp fragment of the *PpMTA* and *PpFIP37* genes using WT plant DNA as a template was amplified by PCR (Table S1), these 2000 bp fragments contain the native sequence in the central position, with 1000 bp on each side, to restore the mutation present in *Ppmta* and *Ppfip37* mutant lines. Also, we added a *de novo* restriction site in these fragments using the PCR Overlap Extension technique, to distinguish a WT plant from a complemented plant. The substitutions generate a silent mutation to preserve the original WT amino acid sequence. For the 2000 bp fragments of *PpMTA* and *PpFIP37* a new SacI and SalI restriction sites were generated, respectively. These fragments were cloned into pJET2.1 (Thermo Fisher Scientific, Walthan, MA) and sequenced to confirm their integrity. The resulting constructs were linearized and transfected as previously described into protoplasts isolated from *Ppmta* and *Ppfip37* single mutant plants to induce homologous recombination. The resulting complemented plants were analyzed by PCR and confirmed by DNA sequencing.

Molecular Characterization of Transgenic lines

Total RNA was isolated from plants of different ages as described in the text. We used the RNeasy Plant Mini kit (QIAGEN, Valencia, CA) and treated the recovered RNA with DNaseI (Thermo Fisher Scientific). cDNA was synthesized from 250 ng DNase-treated RNA using RevertAid Reverse Transcriptase (Thermo Fisher Scientific). The PCR reactions (20 µl) were performed using 1 µl of cDNA template. The primers used for the PCR were designed to amplify 150-200 bp fragments (Table S1).

Dot-blot experiments to immuno-detect m^6A were performed using polyA+ RNA extracted with oligo-dT Dynabeads (Dynabeads mRNA direct purification kit, Thermo Fisher Scientific), as described by the provider. For each sample, 50 ng and 200 ng were used. The RNA samples (5 µl) were denatured by adding 1.6 µl of 4X RNA Denaturing Buffer (16.4 M Formamide, 2.8 M Formaldehyde, 26.6 mM MOPS Buffer [6.7 mM sodium acetate], 1.3 mM EDTA) and incubated at 65 °C for 5 min, cooled on ice, and 6.6 µl of 20X SSC Buffer (3.0 M NaCl, 0.3 M Sodium Citrate, pH 7.0) and 6.7 µl of nuclease-free water, were added. Samples were spotted on a Hybond-N+ membrane (Amersham), previously placed in a 96-well dot blot apparatus (Schleicher & Schuell BioScience, NH). Vacuum pressure was applied to draw the solution through the membrane. After air drying for 5 min, the membrane was UV-crosslinked (2 × auto-crosslink, 1800 UV Stratalinker, Stratagene) and incubated with blocking buffer (5 % low-fat milk in PBS, 0.1 % Tween 20 (PBS-T)) for 1 h at room temperature, then incubated with N6-mA antibody (1:1,000, Cat. #56593S, Cell Signaling Technology, MA, USA) at 4°C overnight. Membranes were washed with PBS-T three times and then incubated with HRP-linked secondary anti-rabbit IgG antibody (1:5,000, Invitrogen, Carlsbad, CA) for 1 h at room temperature. After three washes with PBS-T, the membrane signal was detected with

SuperSignal West Dura Extended Duration Substrate kit (Thermo Fisher Scientific), and a ChemiDoc Imaging System (Bio-Rad, Hercules, CA).

Anatomical analyses

Assay of protonema growth

Protonema from the *Ppmta*, *Ppfip37* and wild type lines was processed to obtain protoplasts with 3 mL of 2 % Driselase (Sigma D9515-25G) and 9 mL of 8 % D-mannitol solution for 1 h. The protoplasts were filtered and centrifuged for 5 min at 250 x g, and then washed 3 times with 10 mL of 8 % D-mannitol solution. These protoplasts were counted and resuspended in liquid plating media at 10,000 protoplasts/mL, and 100 µL of this solution were plated on cellophane over solid PpNH4 medium supplemented with 0.33 M mannitol. These protoplasts grew for 4 days at 25 °C in an 16 h light/8 h dark photoperiod under white light (80 µmol m^{-2} sec^{-1}), then the plants were transferred to PpNH4 media and grown for 7 days. The protonema of all the lines was imaged using an Olympus SZX7-Zoom stereoscope at 10x magnification to detect chlorophyl autofluorescence. At least thirty plants per line were imaged, growth analysis was measured using Image J and the MorphologyMacroPublicV2.6 command (Bibeau and Vidali, 2014), yielding results for area, and solidity (area/convex hull area). This experiment was repeated independently three times, with 10-15 plants per each of three technical replicates.

Bud and gametophore count

We used 14-d-old plants of the *Ppmta*, *Ppfip37*, *Ppmtb1*, *Ppmtb2*, *Ppmtb1/2* and wild type lines to obtain individual plants from protoplasts. We collected 5 clones of each line to analyze them individually using a Leica DMRA2 microscope (Leica Microsystems) at 40x in bright field, the buds were counted and classified in three different visual categories: early buds (bulb shape), mid buds (heart shape), and late buds (first phyllid and presence of rhizoids). This experiment was repeated independently 3 times.

The number of gametophores per colony was also counted in the different genetic backgrounds, we used 20-d-old plants for this analysis, and gametophores were classified according to the number of phyllids they bore. For this experiment we used 5 colonies per line and each colony was dissected under an Olympus SZX7-Zoom stereoscope. This experiment consisted of three independent biological replicates.

Spore generation and germination

To induce sporulation, 7-d-old protonema tissue was homogenized using a FastPrep®-24 apparatus (MP-Biomedicals, OH, USA) and grown in peat moss substrate (Jiffy-7, Jiffy Products International, Stange, Norway), in Magenta boxes filled up with 150 mL water, under sterile conditions. These plants were maintained for 8 weeks at 25 °C in a 16 h light / 8 h dark photoperiod, and then changed to 15 °C in an 8 h light / 16 h dark photoperiod for 4 weeks. Sporophytes were harvested under an Olympus SZX7-Zoom stereoscope, and we calculated the percentage of sporangia at different developmental stages (designated as S1, S2, S3, S4 and MS, see Figure 3B legend for further details).

Germination assays were performed using spores from at least 3 age-matched sporangia from the mature developmental stage (MS). Mature sporangia were bleached in 1 mL 25 % Bleach for 10 min and then washed three times in 1 mL sterile water for 10 min each time, under sterile conditions. The sporophytes were then crushed in 500 µl of sterile water to release the spores, and 100 µl of this spore suspension were diluted in 900 µl of sterile water to plate 1 mL of spore solution per Petri dish. Spores were plated on cellophane overlaid PpNH4 medium, supplemented with 10 mM $CaCl_2$. Plates were air-dried in a laminar flow hood, sealed with micropore tape, and placed at 22 °C in a 16 h light / 8 h dark photoperiod. Spore germination was counted daily using an Olympus SZX7-Zoom stereoscope. A spore was defined as having germinated as soon as the first deformation of the spore coat by the emerging protonemal apical filament was observed. Two to three technical replicates were performed for each of three independent biological replicates. Data were expressed as percentage germination: (germinated spores/total spores counted) x 100.

m^{6}A-IP-RT-PCR

In order to enhance the yield of mRNA recovered from buds, we implemented a reported protocol (Johri and Desai, 1973) that uses naphthalene acetic acid (NAA) and kinetin (Sigma-Aldrich, St. Louis, MO) treatment to induce ~12 times more buds compared with untreated plants. Wild-type plants regenerated from protoplasts were grown in PpNH4 medium for 10 d under normal conditions and then transferred to PpNH4 supplemented with 1 µg/mL of NAA and grown for 5 d, then the plants were transferred to PpNH4 supplemented with 1 µg/mL of Kinetin for 1 d under normal conditions. To collect tissue, first excess moisture was removed with a sterile paper towel, and then it was homogenized to a fine powder using a mortar and pestle cooled with liquid nitrogen. The mRNA was isolated using the Dynabeads mRNA direct purification kit as described by the provider. The m^{6}A-IP assay was performed as previously described (Dominissini *et al.*, 2013) with minor modifications. Briefly, we used 5 µg of mRNA (isolated as previously described) to perform an m^{6}A-IP using an m^{6}A-specific antibody (Cell Signaling Technology). For the m^{6}A-IP-RT-PCR assays, we performed the RNA immunoprecipitation without fragmenting the mRNA. We obtained the immunoprecipitated fraction (m^{6}A fraction) as well as the unbound fraction (non-m^{6}A fraction). These fractions plus the input mRNA were reverse transcribed using Revertaid reverse transcriptase (Thermo Fisher Scientific) with dT primer, and different transcripts were analyzed by semi-quantitative PCR.

MeRIP-seq

Approximately 5 µg of mRNA were extracted using the Dynabeads mRNA direct purification kit (Thermo Fisher Scientific) from plants that were under NAA and kinetin treatment as previously described. The mRNA was treated with the Fragmentation buffer (10 mM Tris-HCl pH 7.0, 10 mM $ZnCl_2$) to obtain ~200 nt fragments. An aliquot of fragmented RNA was saved as input control, and the remainder was incubated with m^{6}A antibody (ab151230, Abcam, Cambridge, UK), in 1x IP buffer (0.2M Tris-HCl. pH 7.4, 1M NaCl, 2 % igepal CA630) supplemented with RiboLock RNase Inhibitor (Thermo Fisher Scientific) overnight at 4 °C. The antibody-bound RNA was then incubated with pre-blocked protein-A magnetic beads (Invitrogen) at 4 °C for 2 h with constant rotation. The immunoprecipitated RNA was released

using an elution buffer (1x IP buffer supplemented with 6.7 mM N6-methyladenosine, Sigma-Aldrich), and purified using ethanol precipitation. The resulting RNA samples were subjected to high-throughput sequencing in an Illumina NextSeq 500 sequencer (Illumina, San Diego, CA) at the Unidad Universitaria de Secuenciación Masiva y Bioinformática, IBT-UNAM. Low-quality reads and adapters were removed from > 13 million total reads per sample using trim_Galore (v. 0.4.1). Mapping to the *P. patens* genome v3.3 available at Phytozome (https://phytozome.jgi.doe.gov/) was performed using Bowtie2 (v.2.2.9, Langmead and Salzberg, 2012), allowing a single mismatch (mapping rate > 76 %). Reads were PCR de-duplicated using Picard tools. Narrow peak calling was performed using MACS2 (v 2.1.1.20160309, Zhang *et al.*, 2008) with a haploid genome length of 475 Mbp, and only peaks with a *p-value* lower than 0.05 were kept. The full peak sequence was used for *de-novo* motif discovery using the meme-suite (v.5.4.1, Bailey *et al.*, 2015). The NGS raw data reported in this work has been deposited to the NCBI database as series GSE213348.

RNA-seq

Protonemal tissue from wild type and *Ppmta* plants that were subjected to NAA and kinetin treatment (as described above) was collected to isolate total RNA using the RNeasy Plant Mini Kit (QIAGEN) and the integrity of the RNA was measured with a Bioanalyzer 2100 (Agilent Technologies, Santa Clara, CA). cDNA libraries were obtained using the True-Seq stranded mRNA Library Prep kit (Illumina) and sequenced using a NextSeq 500 platform (Illumina) with a configuration of 2 × 75 paired-end sequences (Unidad Universitaria de Secuenciación Masiva y Bioinformática, IBT-UNAM). Low-quality reads were removed as mentioned above from at least 30 million total reads per library and mapped to the *P. patens* genome v3.3 available at Phytozome with at least 72 % mapping efficiency. Differential expression analysis was carried out using EdgeR (Robinson *et al.*, 2010), only genes that showed a significant change (corresponding to *p*-value <0.001, logFC >0.5, and FDR <0.01, values from EdgeR) were retained for downstream analysis. We carried out a Gene Ontology (GO) enrichment analysis using ShinyGO with default settings (Ge *et al.*, 2020). Correspondence between MeRIPseq and RNAseq analyses was performed using bedtools (v. 2.25.0). To test for the significance of the set of 79 genes that showed an overlap between RNA-seq and MeRIP seq, we used the set of 2270 genes showing m^6A methylation and obtained 1000 sets of 1000 randomly selected genes, to estimate the probability of overlap by chance. On average, this test returned 36 genes (*p*-value= 3.4e-06 using a Student t-test). The NGS raw data reported in this work has been deposited to the NCBI database as series GSE213348.

mRNA stability assay

Protonemal tissue from wild-type and *Ppmta* plants was subjected to NAA treatment for 4 d (as previously stated). After one day on PpNH4 medium supplemented with 1 µg/mL Kinetin, the plants were transferred to PpNH4 medium containing 10 µM Actinomycin D or DMSO (mock treatment). Total RNA was extracted from tissue collected after 0, 2, 4, 6, and 12 h of treatment using the QIAGEN RNeasy Plant Mini Kit (QIAGEN) and subjected to DNaseI digestion. After cDNA synthesis, the accumulation of different transcripts was examined by RT-qPCR using the gene-specific primers listed in Table S1.

RESULTS AND DISCUSSION

The m^{6}A Methyl Transferase Complex is conserved in *Physcomitrium patens.*

In the genome of *P. patens,* we identified genes that have high percentage of identity with MTC core genes previously identified in *A. thaliana*, used here as reference. We selected *PpMTA* (Pp3c1_32590V3.1, 70 % identity with Arabidopsis MTA) and *PpFIP37* (Pp3c8_10480V3.1, 69 % identity with Arabidopsis FIP37) annotated as putative orthologous genes of *MTA* (Zhong et al, 2008) and *FIP37* (Shen et al., 2016). A recent report (Yue *et al.*, 2019) where the authors used sequence information from 15 land plant species and 7 algae species to identify homologs of the m^{6}A machinery confirmed that the two *P. patens* genes we selected, *PpMTA* and *PpFIP37*, are the most certain orthologs of *MTA* and *FIP37*, respectively. We generated mutant lines for these two genes using the CRISPR/Cas9 technology previously reported in *P. patens* (Lopez-Obando *et al.*, 2016). In the recovered lines, we confirmed the presence of a mutation caused by nucleotide deletions in these loci by genomic PCR and sequencing (diagrams showing the mutations obtained are presented in Figure S1). To confirm that subsequent results are due to the absence of the m^{6}A-MTC activity instead of potential Cas9 off-target artifacts, we generated the complemented lines: PpMTA-C and PpFIP37-C. In these two lines, the mutation was replaced with the native sequence using homologous recombination. The identity of the complemented lines was confirmed by PCR and sequencing of the relevant gene region to confirm their WT sequence. First, we tested for the presence of a transcript in all mutant and complemented plants using RT-PCR (Figure 1a). We observed an absence of transcript accumulation in the *Ppmta* and *Ppfip37* mutant lines when compared with the WT line (likely due to premature stop codons present in the mutant genes, see Figure S1); by contrast, the PpMTA-C and PpFIP37-C lines showed a recovery of the corresponding transcript, similar to the accumulation detected in the WT line. To address if the presence of m^{6}A in mRNA is affected in the mutant lines, we performed a dot blot assay using poly-A+ RNA and incubated it with an antibody which recognizes the m^{6}A modification (Figure 1b). We observed a severe reduction of the m^{6}A signal in the *Ppmta* and *Ppfip37* mutant lines when compared to the WT sample, furthermore the m^{6}A signal was recovered in the PpMTA-C and PpFIP37-C lines. These results confirm that *PpMTA* and *PpFIP37* are the orthologous genes of the Arabidopsis MTC components, however in contrast with Arabidopsis, the mutant *P. patens* plants do not show a lethal phenotype during gametophytic growth and can be maintained by protonema propagation indefinitely.

PpMTB1 and PpMTB2 are essential for m^{6}A addition to mRNA

In addition to *PpMTA* and *PpFIP37*, we identified two proteins PpMTB1 and PpMTB2 (Pp3c5_5900V3.1 and Pp3c6_26980V3.1, respectively) that share high percentage of identity (81% and 67% respectively) with *MTB*, the Arabidopsis ortholog of METTL14. The same genes were previously identified as potential orthologs of *MTB* (Yue *et al.*, 2019). Nevertheless, in those organisms where m^{6}A addition has been reported, the METTL14

protein, an essential factor of the MTC, is always encoded by a single gene. We generated single and double mutants for the *PpMTB1* and *PpMTB2* putative genes using CRISPR-Cas9 genome editing. We obtained mutations that resulted in the formation of a premature stop codon in the *Ppmtb1* and *Ppmtb2* single mutants (Figure S1). The accumulation of the corresponding transcripts, analyzed by RT-qPCR, showed a drastic reduction in the single mutants, likely due to the presence of the premature stop codon (Figure 1c). Then, we analyzed the presence of m^6A in poly-A+ RNA by performing a dot blot assay. We observed that the single mutants displayed an m^6A signal similar to that of the WT plants (Figure 1d). Thus, we obtained a *Ppmtb1*/*Ppmtb2* double mutant line carrying the same alleles as the single mutants which showed a significant reduction of the m^6A signal, similar to that of the *Ppmta* mutant (Figure 1d). This result indicates that *PpMTB1* and *PpMTB2* genes are both active and could function redundantly in m^6A catalysis in *P. patens*, raising the possibility that the heterodimer with PpMTA within the MTC might be assembled in some cases with PpMTB1 and in other cases with PpMTB2, adding a new layer of complexity to the m^6A catalysis in *P. patens*.

Loss of m^6A function causes a delay in gametophore bud development

Having established the molecular defects caused by mutations in the genes encoding for the core components of the MTC complex, we analyzed the effects of the absence of m^6A catalysis throughout the life cycle of *P. patens*. First, we evaluated the growth of the protonema, to do so, we obtained protoplasts from 7-day-old protonema from *Ppmta*, *Ppfip37*, a quadruple mutant (QM: *Ppmta*/*Ppfip37*/*Ppmtb1*/*Ppmtb2*) and wild type plants. After 7 days of growth on PpNH4 medium, no significant difference in plant area was observed among the mutant lines when compared to that of the wild type plants (Figure S2), suggesting that at this developmental stage, m^6A presence in mRNA is not essential, allowing the protonema to be continuously propagated.

Next, we explored the formation of gametophore buds. For this experiment we obtained protoplasts from 7-day-old protonema from *Ppmta*, PpMTA-C, *Ppfip37*, PpFIP37-C and wild type plants and after 14 days of growth the number of buds was counted and classified in three different visual categories: early buds (bulb shape), mid buds (heart shape), and late buds (first phyllid and presence of rhizoids, see Figure S3). The total number of gametophore buds and those progressing to the late developmental categories were dramatically reduced in the mutant lines (Figure 2a). These phenotypes are clearly associated to the absence of m^6A catalysis as the complemented lines showed a number of gametophore buds with a maturity distribution similar to that of the wild type plants (Figure 2a). The mutant phenotypes of reduced bud number and the reduction of late buds could be associated to a lower production, or alternatively, to a delay in their formation. To further dissect this phenotype, we counted the number of gametophores in 20-d-old plants, and we classified them based on the number of phyllids they bore. The *Ppmta* and *Ppfip37* mutant lines showed a reduced number of gametophores with a smaller number of phyllids in comparison with PpMTA-C, PpFIP37-C and the wild type lines, which had gametophores that bore up to eight phyllids (Figure 2b, and 2c). Importantly, bud development continued over time in all genetic backgrounds, as evidenced by the number of resulting gametophores in 20-d-old plants (compare number of buds in Figure 2a to number of gametophores in Figure 2b).

However, the mutant lines displayed buds and gametophores mainly at younger developmental stages. Together, these results indicate that the reduced number of buds and gametophores observed in the mutant lines is not due to an arrest in their growth, but instead is consistent with a delay in developmental progression, and that this phenotype is dependent on m^6A catalysis.

These features were also evaluated in the *Ppmtb1*, *Ppmtb2* and *Ppmtb1*/*Ppmtb2* lines. In this case we did not observe any obvious defect in the *Ppmtb1* and *Ppmtb2* single mutant lines. Nevertheless, the *Ppmtb1/Ppmtb2* double mutant displayed a decrease in the number and maturity of buds and gametophores comparable to those obtained with the *Ppmta* mutant (Figure 2d-2f). These results indicate that *PpMTB1* and *PpMTB2* are necessary for correct bud and gametophore formation. Moreover, this requirement, together with the reduced m^6A level in mRNA observed only in the double mutant (see Figure 1d), suggests that *PpMTB1* and *PpMTB2* act redundantly, at least during these developmental stages.

So far, we identified the main components of the MTC described in other species. The mutants of the *PpMTA*, *PpFIP37*, *PpMTB1* and *PpMTB2* genes show reduced levels of m^6A modification on mRNA and similar phenotypic defects during bud and gametophore development, suggesting they are involved in the regulation of the transition from protonema to gametophore bud formation. Consistently, when we evaluated the expression of the MTC core genes in a previous RNA-seq analysis of bud cells and protonemal apical cells collected separately by laser microdissection (Frank and Scanlon, 2015), we observed that the *PpMTA*, *PpFIP37*, *PpMTB1* and *PpMTB2* transcripts showed an abundant accumulation specifically in bud cells (refer to Table S1 in Frank and Scanlon, 2015), correlating with the contribution of the m^6A modification of mRNA to gametophore bud formation.

The development and viability of spores is affected in the MTC mutant plants

To extend the phenotypic analysis throughout the life cycle of *P. patens* and uncover other effects due to the absence of m^6A catalysis, we evaluated the development of the spores and their viability. To this end, we examined *Ppmta*, *Ppfip37*, *QM* and wild type plants. For this experiment, we considered the delay previously observed in the development of buds in the mutants, to let the plants grow for 8 weeks instead of 6 weeks under standard conditions (25 °C in a 16 h light / 8 h dark photoperiod), allowing the different plant lines to produce as many gametophores as possible, before the induction of gametangia development (15 °C, 8 h light / 16 h dark). We collected all the sporangia 4 weeks post-induction and classified them into different maturation stages according to their morphological features (e.g., size, shape, and color, Figure 3a). All mutant lines showed a lower percentage of mature sporangia (12-20 %) than that of the wild type plants (46 %, Figure 3b), indicating that m^6A modification of mRNA participates in sporangium development in *P. patens*. Considering that the publicly available expression datasets indicate that the major accumulation of the transcripts encoding for the MTC proteins occurs during the development of the sporophyte, and specifically in the mature spore (Figure S4, eFP Browser, http://bar.utoronto.ca/efp_physcomitrella/cgi-bin/efpWeb.cgi), we focused on the morphology and viability of the spores. We evaluated the spores obtained only from mature sporangia and analyzed their size, morphology, and viability. The spores of all the mutant

lines tested exhibited a strong reduction in their size (Figure 3c and 3d), and an abnormal shape, observing a flattened shape that is completely different in morphology from the regular round shape observed in the wild type spores (Figure 3e). Lastly, we evaluated the germination rate of the spores isolated from *Ppmta*, *Ppfip37*, QM and wild type plants. We observed that the spores of all the mutant lines were unable to germinate while the spores of wild type plants reached the highest percentage of germination at 10 days (Figure 3f). These results reveal that the components of the MTC are also required for the proper development and germination of the spores; consequently, MTC absence leads to a lethal phenotype preventing the life cycle of *P. patens* to be completed. This phenotype resembles that of the embryonic lethality observed in Arabidopsis *mta* and *fip37* mutants, in which the mutant embryos exhibit a developmental arrest during the globular stage, where normally the embryo undergoes asymmetrical cell divisions leading to the establishment of the 3D pattern (Shen *et al.*, 2016; Zhong *et al.*, 2008). The molecular mechanisms regulating zygote development in *P. patens* life cycle, are not understood. While there are clear differences between the 3D growth of the sporophyte and the 3D growth occurring during gametophore bud formation, it remains unknown whether these two processes share similar factors, in part because most of the mutants affected in 3D growth patterning do not form gametophores and in consequence the development of the sporophyte cannot be analyzed (Aoyama *et al.*, 2012; Moody *et al.*, 2018; Perroud *et al.*, 2014). Future work in *P. patens* will help uncover the role of MTC factors in these developmental steps.

Identification of m^{6}A-modified mRNAs revealed that all *PpAPB* transcripts are methylated

Here, we demonstrate that the m^{6}A pathway plays a relevant role in the development of the spores and their germination, however due to the lack of information on the molecular pathways underlying this process, we decided to first evaluate the molecular contribution of the m^{6}A mRNA modification to the metabolism of the transcripts during the transition from protonema to gametophore bud development. For this, we identified the m^{6}A-modified transcripts using 18-d-old wild type plants treated with NAA and kinetin, a means used to increase the number of buds and therefore magnify the signal originating from the bud-specific transcriptome. Because the MeRIP-Seq analysis has not been employed before in *P. patens* plants at this growth stage, we first tested the suitability of the m^{6}A-antibody. For this purpose, we performed an m^{6}A-immunoprecipitation assay and analyzed the accumulation of some transcripts by RT-PCR in the different fractions obtained: initial poly-A+ RNA (input), immunoprecipitated fraction (m^{6}A) and unbound fraction (non-m^{6}A). To ask if some of the mRNAs encoding for factors involved in bud development are m^{6}A-modified, we selected a potential ortholog of the mitogen-activated protein kinase kinase *YODA* mRNA, which in Arabidopsis is methylated (Shen *et al.*, 2016), and highly accumulated in bud cells (Frank and Scanlon, 2015). We also included *DEK1*, and *PpAPB1*, which are central factors in the developmental pathway of gametophore buds, and as negative controls we selected *UBI10* and *ACT7* because no methylation of these mRNAs has been described. From this analysis we observed that *PpAPB1* and *PpYDA*, the putative ortholog of *YODA* were enriched in the m^{6}A fraction, whereas *ACT7*, *UBI10* and *DEK1* were mainly enriched in the non-m^{6}A fraction (Figure 4a), demonstrating that the antibody has the specificity required to discriminate

among transcripts, and indicating its selectivity to immunoprecipitate m^{6}A-modified mRNAs. Consequently, we performed a MeRIP-seq analysis to identify methylated mRNAs at the transcriptome level. We identified 2532 methylation peaks spread over 2270 transcripts, indicating that some of these have more than one methylation peak (Table S2). The m^{6}A peaks were enriched near the stop codon and to a lesser extent towards the start codon (Figure 4b), an observation that has also been reported in other plant species (Luo *et al.*, 2014; Xu *et al.*, 2021). By applying the MEME algorithms to identify potential methylation sequence motifs enriched in these regions. Hence, we found a 7-nt sequence with the consensus GRAGRAG (where R= A/G, *p*-value= 9.1e-056, Figure 4c). Previous reports have shown that in plants the methylation motif RRACH has undergone diversification, and furthermore, depending on the tissue, growth conditions or environmental stimuli, the modified mRNAs exhibit different consensus motifs (Anderson *et al.*, 2018; Govindan *et al.*, 2022; Zhou *et al.*, 2022). Here, we propose GRAGRAG as a novel methylation motif present in *P. patens* during bud formation, however, it is necessary to carry out additional tests to confirm the functionality of this motif and define which adenosine is being methylated within this consensus sequence.

Next, we performed a Gene Ontology (GO) analysis of the 2270 transcripts identified by MeRIP-seq, revealing an enrichment of several RNA metabolism-related categories, while no obvious association to bud development was recognized (Figure S5). Importantly, we found that *PpAPB1* and *PpAPB2* mRNAs are present in our MeRIP-Seq analysis (Figure 4d). Because of this finding, we examined whether *PpAPB3* and *PpAPB4* mRNAs are also methylated. To do so, we performed an m^{6}A-IP-RT-PCR assay and confirmed that *PpAPB2*, *PpAPB3* and *PpAPB4* mRNAs are enriched in the m^{6}A fraction, indicating that all four *PpAPB* transcripts can be m^{6}A-modified (Figure 4a and 4e). In contrast to *PpAPB1* and *PpAPB2*, the mRNAs for *PpAPB3*, *PpAPB4* and *PpYDA*, the putative ortholog of *YODA*, which we detected in our m^{6}A-IP-RT-PCR, were not found in the MeRIP-seq analysis as high-confidence candidates. This result could be explained by the fact that we did not specifically employ tissues originating from bud cells, and the m^{6}A signal from the bud-specific transcripts could have been diluted. Alternatively, the MeRIP-seq assay may underestimate the abundance of m^{6}A-modified mRNAs with low expression levels (Dominissini *et al.*, 2013; Shen *et al.*, 2016) and thus, other important m^{6}A-modified transcripts may remain to be discovered. Nonetheless, the presence of m^{6}A in all four *PpAPB* mRNAs could affect their metabolism and in consequence contribute to gametophore bud development and be consistent with the phenotype observed in the MTC mutants during the developmental transition from protonema to gametophore buds. To investigate the relationship between the presence of m^{6}A in mRNA and its accumulation, we analyzed the molecular defects caused by its absence in the *Ppmta* mutant.

The metabolism of several m^{6}A-modified mRNAs is affected in the *Ppmta* mutant

To further examine the global effect of m^{6}A addition on mRNA in the *P. patens* transcriptome during the transition from protonema to gametophore buds, we performed an RNA-seq analysis to compare the *Ppmta* mutant and the wild type transcriptomes. To this end, we employed 18-d-old plants of both genotypes treated with NAA and kinetin, to increase bud formation, as described before. We identified 1081 differentially expressed (DE) transcripts,

including 520 down-regulated and 561 up-regulated genes (Figure S6 and Table S3). When we searched for enriched GO categories using these DE transcripts, we could not detect any directly related to gametophore bud development, but mostly others associated with metabolic processes, likely a consequence of developmental activity (Figure S6). Next, to investigate the direct effect of the m^{6}A modification on gene expression during this developmental stage, we compared the results of the RNA-seq and MeRIP-seq analyses, where we identified 79 DE mRNAs that were also m^{6}A modified (Figure 5a and Table S4). We first arranged these 79 recovered transcripts according to their differential expression, from up- to down-regulated (33 and 46 mRNAs, respectively). When we observed the extent of methylation in each mRNA (as defined by the *p*-value), there was no clear association between this value and the direction of changes in mRNA accumulation (Figure 5a), suggesting that additional factors determine the fate of the m^{6}A-containing transcripts to direct them to down- or up-regulation as described in other biological systems (Frye *et al.*, 2018; Ivanova *et al.*, 2017; Wang *et al.*, 2021), including plants (Anderson *et al.*, 2018; Govindan *et al.*, 2022). Among these 79 m^{6}A-DE transcripts, we identified factors involved in the development of buds, for instance: *PpAPB2* (Pp3c9_25570) (Aoyama *et al.*, 2012), and others related to auxin signaling such as ARF domain protein (Pp3c6_21370V3.1) and AUX/IAA domain factor (Pp3c15_9710V3.1), which are methylated and down-regulated in *Ppmta* plants (indicated by aqua asterisks in Figure 5a, 5c, and Figure S7a). Furthermore, we performed a GO analysis using only these 79 m^{6}A-DE transcripts, where we identified processes related to the development of gametophore buds, including categories such as shoot system development, multicellular organism development and post-embryonic development (indicated by purple asterisks in Figure 5b). Among the mRNAs comprised in these categories, we recognized the presence of SNF1 Kinase Interactor-like protein (Pp3c16_25700), Epidermal Patterning Factor-like protein (Pp3c23_5720), Inosine-uridine Preferring Nucleoside Hydrolase (Pp3c26_14640) and UDP-glucuronate 4-epimerase (Pp3c11_14370) (indicated by red asterisks in Figure 5a, and Figure S7b). However, their participation during bud development has not been studied, and therefore their analysis can add new clues and enlighten the molecular mechanisms underlying the transition from protonema to gametophore buds, through the regulation of their mRNA metabolism due to m^{6}A addition.

Loss of m^{6}A affects the stability of *PpAPB* transcripts

As shown above, we identified *PpAPB2* as a m^{6}A-DE mRNA, and the loss of m^{6}A is associated with a decrease in its accumulation in *Ppmta* plants (Figure 5a). Moreover, we showed that all the *PpAPB* transcripts are methylated (Figure 4a and e), thus we analyzed the mRNA accumulation of *PpAPB1*, *PpAPB3* and *PpAPB4* in the *Ppmta* plants. The RNA-seq analysis showed that they tend to be down-regulated in the mutant plants (Figure 5c), suggesting that m^{6}A is important to allow the appropriate accumulation levels of these transcripts. However, it is necessary to directly test whether this reduction is due to the absence of m^{6}A. In this respect, one of the principal mechanisms that m^{6}A employs to facilitate the turnover of the transcriptome is by offering stability to transcripts that are important for the establishment of the new cellular stage. To assess this possibility, we employed actinomycin D to inhibit global transcription in *Ppmta* and wild type plants and measured the mRNA

accumulation levels of *PpAPBs* over time (0, 2, 4, 6 and 12 h). Accordingly, in wild type plants all transcripts showed a reduction in their abundance over time, consistent with mRNA turnover. However, all four *PpAPBs* showed a larger decrease in their mRNA levels in *Ppmta* plants, when compared to the levels observed in wild type plants, whereas no difference was observed in a non-methylated transcript (*DEK1*, Figure 6). This result indicates that the presence of m^6A on *PpAPB* transcripts facilitates their correct accumulation during gametophore bud development and the absence of this modification leads to a decrease in their abundance, contributing to the phenotype of delay in bud formation observed for the *Ppmta*, *Ppfip37*, *Ppmtb1*/*Ppmtb2* mutants (see Figure 2). Despite the contribution of m^6A to the stability of *PpAPB* transcripts, it is likely that other factors equally regulated by this modification contribute to the phenotype observed, such as Pp*YDA*, the putative ortholog of *YODA* (Figure 4a and 6), which acts downstream of the *PpAPBs*, offering a bird's eye view of how dynamic and complex is the regulation mediated by this mRNA modification.

CONCLUSION

This study reports on the functions of the m^6A modification on mRNA in a non-vascular plant model, where we identified the main factors of the Methyltransferase complex in *P. patens*. In contrast with other organisms, we identified two functional homologs for MTB, raising the possibility that different MTC complexes are formed to regulate specific substrates in the moss *P. patens*. We demonstrate that the function of the MTC is conserved and that its inactivation by mutation, and therefore the loss of the regulation mediated by m^6A, leads to a delay in the development of gametophore buds and more importantly yields non-viable spores. Both phenotypes resemble those observed in Arabidopsis, where the mutants of the MTC show embryos that fail to divide in three dimensions leading to a lethal phenotype. Furthermore, we identified mRNAs that are methylated during bud development and confirmed that the *PpAPB1-4* transcripts contain m^6A and that this modification facilitates their correct accumulation through the regulation of their mRNA stability. In a broader context, we propose that m^6A is essential to enable the appropriate levels of these and other bud-specific transcripts directing the turnover of stage-specific transcriptomes, and thus promoting the transition from protonema to gametophore buds (Figure 7a). In the MTC mutants, certain bud-specific transcripts are devoid of the regulation mediated by m^6A, thus failing to reach proper RNA levels, causing a delay in gametophore bud development (Figure 7B). The innovation of 3D growth in the development of plants coincides with a series of other novelties in their evolution, for instance: the origin of extracellular matrices (sporopollenin, cellulose, lignin, and pectin, among other compounds), the establishment of intercellular communication networks (plasmodesmata, phytohormone signaling) and the diversification of gene regulatory networks to promote cell differentiation (Bowman *et al.*, 2007; Wickett *et al.*, 2014), suggesting that m^6A gained prominence in the regulation of other aspects of plant development requiring a transcriptome turnover. These features were acquired early in the evolution of plants and are conserved in flowering plants, opening new avenues to better understand how the m^6A modification of mRNA contributes to the

evolution and regulation of 3D growth patterning and other important processes in plant development.

ACKNOWLEDGMENTS

DGM was supported by a scholarship (817571) from Consejo Nacional de Ciencia y Tecnología, México. We acknowledge the work of Selene Fernández from LANGEBIO-IPN for the initial analysis of the MeRIP-seq data. We also thank Ma. Beatríz Pérez Morales for her excellent technical support during the development of this work. This work was partially supported by grants from DGAPA-PAPIIT (IN-208421) and CONACyT (FC-2015-184) to JLR. The IJPB benefits from the support of Saclay Plant Sciences-SPS (ANR-17-EUR-0007).

AUTHOR CONTRIBUTIONS

DGM performed experiments, analyzed data, and wrote the first draft of the manuscript. FC and FN generated mutant lines, VMP performed bioinformatic analyses, AAC contributed to data analysis, discussion, and manuscript preparation. FN and JLR conceived this project, JLR supervised the project, analyzed data, and coordinated manuscript preparation. All authors contributed to manuscript writing and approved the final version.

DATA STATEMENT

The NGS raw data reported in this work has been deposited to the NCBI database as series GSE213348.

CONFLICT OF INTEREST

The authors have declared no conflicts of interest for this article.

FIGURE LEGENDS

Figure 1. Mutation of the MTC genes affects m^{6}A addition to mRNA.
(a) Total RNA was isolated from *Ppmta*, *Ppfip37*, complemented lines (PpMTA-C and PpFIP37-C), and wild type plants (2-week-old), and subjected to RT–PCR to evaluate the presence of the corresponding transcripts (*PpMTA* indicated in red and *PpFIP37* in blue). NC MTA and NC FIP37 correspond to PCR negative control samples. **(b)** A dot-blot immuno-assay was employed to detect m^{6}A levels in poly-A+ RNA isolated from wild type, *Ppmta*, PpMTA-C, *Ppfip37*, and PpFIP37-C plants 2-week-old. Two different amounts of poly-A+ RNA were used in each case (50 and 200 ng). **(c)** Total RNA was isolated from wild type, *Ppmtb1*, and *Ppmtb2* plants, and subjected to RT–qPCR to evaluate the abundance of the corresponding

transcripts. The mRNA for *ACT7* was used as reference gene. Statistical significance was evaluated with a T-test (**** p<0.001). Error bars represent standard deviation for two independent biological samples with three technical replicates each one. **(d)** A dot-blot immuno-assay was performed to detect m^6A levels in poly-A+ RNA isolated from wild type, *Ppmtb1*, *Ppmtb2*, *Ppmtb1*/*Ppmtb2 double mutant,* and *Ppmta* plants. Two different amounts of poly-A+ RNA were used for each sample (50 and 200 ng).

Figure 2. Mutants of the MTC genes show a delay in the development of gametophore buds.
(a) Fourteen-day-old plants were dissected to visualize gametophore buds that were visually classified into three different stages of growth (early, mid and late). Five plants of each genotype (wild type, *Ppmta*, PpMTA-C, *Ppfip37*, and PpFIP37-C) were counted for each of three independent biological replicates. Statistical significance was evaluated using ANOVA (**** p<0.001). Error bars represent standard deviation. **(b)** Twenty-day-old plants were dissected to visualize gametophores that were classified according to the number of phyllids they bore. Five plants of each genotype (wild type, *Ppmta*, PpMTA-C, *Ppfip37*, and PpFIP37-C) were counted for each of three independent biological replicates. Statistical significance was evaluated using ANOVA (**** p<0.001). Error bars represent standard deviation. **(c)** Individual plants from the different genotypes evaluated in (b) as seen under the stereoscope. Black arrow heads indicate the presence of gametophores in wild type plants as a reference, scale bar= 5 mm. **(d)** Fourteen-day-old plants were dissected to visualize gametophore buds that were classified into three different stages of growth (early, mid and late). Five plants of each genotype (wild type, *Ppmtb1*, *Ppmtb2*, *Ppmtb1*/*Ppmtb2 double mutant,* and *Ppmta*) were counted for each of three independent biological replicates. Statistical significance was evaluated using ANOVA (**** p<0.001). Error bars represent standard deviation. **(e)** Twenty-day-old plants were dissected to visualize gametophores that were classified according to the number of phyllids they bore. Five plants of each genotype (wild type, *Ppmtb1*, *Ppmtb2*, *Ppmtb1*/*Ppmtb2 double mutant,* and *Ppmta*) were counted for each of three independent biological replicates. Statistical significance was evaluated using ANOVA (**** p<0.001). Error bars represent standard deviation. **(f)** Individual plants from the different genotypes (wild type, *Ppmtb1*, *Ppmtb2*, *Ppmtb1*/*Ppmtb2 double mutant,* and *Ppmta*) analyzed in (e) were grown for another 10 d (1-month-old) and seen under the stereoscope to better show gametophores. Scale bar= 5 mm.

Figure 3. Disruption of m^6A addition triggers aberrant spore phenotypes.
(a) Sporangia were observed under a stereoscope and the different growth stages were visually classified into five categories: Stage 1 through 4 (S1-S4) and Mature Sporangia (MS). Scale bar= 500 mm. **(b)** Sporangia were counted from wild type, *Ppmta, Ppfip37* and *QM (Ppmta*, *Ppfip37, Ppmtb1*, *Ppmtb2*) plants, classified according to the different growth stages as S1-S4 or MS, and represented as percentage of total. Between 144 and 163 sporangia were collected from all the plants grown in three magenta boxes per each of three independent experiments. **(c)** Spores from mature sporangia (MS) from each genotype

analyzed in (b) were photographed (scale bar= 25 μm) to calculate area. A total of 150 spores were collected in each of three independent experiments. **(d)** Measurement of spore area for each genotype as indicated. Statistical significance was evaluated using ANOVA (**** p<0.001). **(e)** representative spores from wild type and *QM* plants were observed using multiphotonic confocal microscopy, scale bar= 25 mm. **(f)** Mature spores from wild type, *Ppmta, Ppfip37* and *QM* plants were tested for germination efficiency in PpNH4 medium supplemented with 10 mM $CaCl_2$ and incubated for as long as indicated in the figure. Germination of at least 250 spores was counted for each of three technical replicates of three independent biological experiments. Error bars represent standard deviation.

Figure 4. The transcripts of PpAPBs are methylated and detected by MeRIP-seq in bud-enriched plants.

(a) Poly-A+ RNA was isolated from 18-d-old wild type plants treated with NAA (1 μM) for 5 d and then kinetin (1 μM) for 1 d. A fraction of the recovered RNA was saved (input, shown in green) and the remaining was used for immunoprecipitation using the anti-m^6A antibody (m^6A fraction, shown in red), and the unbound fraction was also recovered (no-m^6A, in blue). The three fractions were subjected to RT–PCR to evaluate the presence of different transcripts, as indicated. NG= negative control of PCR reaction. **(b)** Distance distribution of m^6A-containing peaks identified by MeRIP-seq, towards start or stop codons. **(c)** The MEME suite of algorithms was used to identify potential conserved motifs in the 2270 peaks obtained from the MeRIP-seq analysis, returning the 7-nt long motif GRAGRAG (R=A/G, p-value= 9.1e-056). **(d)** Diagrams show the gene structure for *PpAPB1* (Pp3c15_24980v3.1) and *PpAPB2* (Pp3c9_25570v3.1). The plots below indicate the position of enriched peaks shown as the $\log^2$ ratio of IP/input (in blue and red bars). **(e)** Poly-A+ RNA from wild type plants was used for m^6A-immunoprecipitation. A fraction of the starting RNA sample was saved (input, shown in green) and the remaining was used for immunoprecipitation using the anti-m^6A antibody (m^6A fraction, shown in red), and the unbound fraction was also recovered (no-m^6A, in blue). The obtained fractions were subjected to RT–PCR to evaluate the presence of *PpAPB2* to 4 and ACT5 transcripts, as indicated. NG= negative control of PCR reaction.

Figure 5. m^6A-modified transcripts show differential expression.

(a) Heat map of the comparison of RNA-seq analysis of *Ppmta* and wild type plants, and MeRIP-seq of poly-A+ RNA of wild type plants showing transcripts according to their differential expression, from up- to down-regulation (left column with $\log^{10}$ fold change indicated), and their corresponding methylation extent (as defined by the p-value). Dotted lines in aqua color indicate the average value of the data and the solid lines show the value for individual genes, as shown in the color and histogram key above. Genes related to bud development are indicated by aqua asterisks. Genes corresponding to GO terms highlighted in (b) are indicated by red asterisks. **(b)** GO analysis of the 79 DE genes obtained in (a) to reveal functional categories. Categories related to developmental processes are indicated by purple asterisks. The size of the dots indicates the number of genes included in each category. Colors represent the $-\log^{10}$ value for false discovery rate (FDR). **(c)** Diagrams show the gene structure for *PpAPB1* (Pp3c15_24980v3.1), *PpAPB2* (Pp3c9_25570v3.1), *PpAPB3* (Pp3c9_25400v3.1) and *PpAPB4* (Pp3c15_24790v3.1). The plots below indicate the position

of m^6A-enriched peaks found by MeRip-seq shown as the log^2 ratio of IP/input (in blue and red bars). The accumulation levels obtained in the RNA-seq replicate 1 and 2 are indicated below as log^2 ratio of *Ppmta*/wt, shown as blue bars (up-regulated) or red bars (down-regulated).

Figure 6. m^6A modification confers stability to PpABP1-4 transcripts.
Eighteen-d-old plants (*Ppmta* and wild type) were treated with NAA (1 μM) for 5 d and then kinetin (1 μM) for 1 d. After this period, plants were further divided in two groups, one treated with actinomycin D (10 μM) and another with mock (DMSO) for 0, 2, 4, 6 or 12 h. Total RNA was isolated from these plants and subjected to RT–qPCR to evaluate the presence of transcripts encoding for *PpAPB1-4*, *PpYDA* putative ortholog, and *PpDEK1*. Results are shown as the value from the Act D samples normalized to mock samples and referenced to the 0 h time point. Error bars represent standard deviation, * = 0.05 *p*-value using a T-test. The analysis was made with two independent biological samples with three technical replicates each.

Figure 7. m^6A modification facilitates the accumulation of bud-specific transcripts to allow the transcriptome turnover required for the 2D to 3D transition.
Working model showing the contribution of m^6A modification of mRNA on transcripts during transcriptome reshaping to facilitate the establishment of gametophore buds from protonema. **(a)** In wild type plants, m^6A addition to mRNAs (shown as red circles) is performed by the MTC, consisting of PpMTA, PpFIP37 and either PpMTB1 or PpMTB2. The presence of m^6A is correlated with the increased stability and ensuing accumulation of certain transcripts, including *PpAPB1-4* and likely other unidentified factors, as shown in the figure. The correct accumulation of stage-specific transcripts secures timely bud development. **(b)** In contrast, in the *Ppmta* mutant line the absence of MTA (or other components in individual mutants) disrupts the addition of m^6A , leading to an impaired accumulation of certain transcripts known to be involved in the development of gametophore buds (such as *PpAPB1-4*) and, in consequence, a delay during this transition is observed.

SUPPLEMENTARY INFORMATION

Figure S1. CRISPR/Cas9 edition of MTC genes caused frameshift mutations
Diagrams show the genomic structure of the *PpMTA*, *PpFIP37*, *PpMTB1* and *PpMTB2* genes analyzed in this work. The annotated protein domains were obtained using NCBI Conserved Domain Search Tool, and are indicated in colors within exons, introns are represented by thin black lines and 5'UTR, and 3'UTR are shown in grey rectangles. MTase: methyl-transferase domain, RRM: RNA-recognition motif. PpMTB1 and PpMTB2 proteins have different domains at their N-terminus, PpMTB1 has the Neuromodulin and the Rho domains, while PpMTB2 has two RRMs. The mutations generated by CRISPR/Cas9 are indicated in the schemes by grey boxes above the genes, the position of the premature stop codon generated by frameshift is shown by a red asterisk. Insertions and deletions caused by genome editing are

indicated for each mutant. PpMTB1 and PpMTB2 alleles present in the quadruple mutant (*QM*) are also indicated.

Figure S2. Early protonema growth is not affected in the MTC mutant lines
Protoplasts of the *Ppmta*, *Ppfip37*, quadruple mutant (*QM*: *Ppmta*, *Ppfip37*, *Ppmtb1* and *Ppmtb2*), and wild type lines were grown in PpNH4 medium for 7 d. The protonema of all the lines was imaged, and growth analysis (in mm^2) was measured using Image J and the MorphologyMacroPublicV2.6 command (Bibeau and Vidali, 2014). Individual plants are represented by black dots, median is shown as a red horizontal line. This experiment was repeated independently three times, with 10-15 plants per each of three technical replicates. ns: non-significant.

Figure S3. Classification of gametophore buds according to developmental stages.
The panels show the different classification of buds identified in 15-day-old plants. **(a)** Early buds are defined as having a bulb shape, **(b)** Mid buds had a heart shape, and **(c)** Late buds were those that had rhizoids. Scale bars, 50 µm. Buds are indicated by a black arrow.

Figure S4. The accumulation of methyltransferase complex transcripts is larger during sporophyte development.
Gene expression maps for **(a)** *PpMTA*, **(b)** *PpFIP37*, **(c)** *PpMTB1* and **(d)** *PpMTB2* were obtained from the eFP browser (http://bar.utoronto.ca/efp_physcomitrella/cgi-bin/efpWeb.cgi). In these schemes we observe the absolute accumulation of the transcripts that encode for the MTC components in *P. patens*. For all of them, the highest expression observed is in the developing sporophyte and in the mature spore.

Figure S5. Gene Ontology categories of m^6A modified transcripts recovered by MeRIP-seq analysis.
Genes that were recovered in the MeRIP-seq analysis were used to identify GO categories using the shinyGO program. Categories are enlisted according to the fold enrichment and the false discovery rate (FDR, in $-\log^{10}$) is shown in a color scale as indicated in the figure. Number of genes included in each GO category are represented by the size of the circle.

Figure S6. Analysis of RNA-seq data obtained from *Ppmta* and wild type plants.
(a) Principal Component Analysis showing the similarity among sequencing libraries, control (in red) and mettl3 (*Ppmta*, in green), replicate libraries 1 and 2 are indicated.
(b) Volcano plots showing differentially expressed genes (DEGs) between *Ppmta* and wild type plants. Red dots represent significant DEGs. Negative $\log^2$ fold change values represent down-regulation, and positive values, up-regulation.
(c) DEGs identified in the RNA-seq analysis were used to identify GO categories using the shinyGO program. Categories are enlisted according to the fold enrichment, and the false discovery rate (FDR, in $-\log^{10}$) is shown in a color scale as indicated in the figure. Number of genes included in each GO category are represented by the size of the circle.

Figure S7. Selected transcripts showing m^{6}A presence and their corresponding differential accumulation in *Ppmta* and wild type plants.

Diagrams show the structure of genes encoding factors related to (a) auxin signaling and (b) others found in development-related GO categories shown in Figure 5B. The plots below each gene indicate the position of enriched peaks found by MeRIP-seq shown as the log^2 ratio of IP/input (in blue and red bars). The accumulation levels obtained in the RNA-seq replicate 1 and 2 are indicated below as log^2 ratio of *Ppmta*/WT, shown as blue bars (up-regulated) or red bars (down-regulated).

REFERENCES

Anderson, S.J., Kramer, M.C., Gosai, S.J., et al. (2018) N6-Methyladenosine Inhibits Local Ribonucleolytic Cleavage to Stabilize mRNAs in Arabidopsis. *Cell Rep.*, **25**, 1146-1157.e3.

Aoyama, T., Hiwatashi, Y., Shigyo, M., Kofuji, R., Kubo, M., Ito, M. and Hasebe, M. (2012) AP2-type transcription factors determine stem cell identity in the moss Physcomitrella patens. *Development*, **139**, 3120.

Arribas-Hernández, L., Bressendorff, S., Hansen, M.H., Poulsen, C., Erdmann, S. and Brodersen, P. (2018) An m ^{6} A-YTH Module Controls Developmental Timing and Morphogenesis in Arabidopsis. *Plant Cell*, **30**, 952–967.

Bailey, T.L., Johnson, J., Grant, C.E. and Noble, W.S. (2015) The MEME Suite. *Nucleic Acids Res.*, **43**, W39-49.

Bibeau, J.P. and Vidali, L. (2014) Morphological Analysis of Cell Growth Mutants in Physcomitrella. In V. Žárský and F. Cvrčková, eds. *Plant Cell Morphogenesis*. Methods in Molecular Biology. Totowa, NJ: Humana Press, pp. 201–213. Available at: http://link.springer.com/10.1007/978-1-62703-643-6_17 [Accessed June 7, 2022].

Bodi, Z., Zhong, S., Mehra, S., Song, J., Graham, N., Li, H., May, S. and Fray, R.G. (2012) Adenosine Methylation in Arabidopsis mRNA is Associated with the 3' End and Reduced Levels Cause Developmental Defects. *Front. Plant Sci.*, **3**, 48.

Bowman, J.L., Floyd, S.K. and Sakakibara, K. (2007) Green Genes—Comparative Genomics of the Green Branch of Life. *Cell*, **129**, 229–234.

Charlot, F., Goudounet, G., Nogué, F. and Perroud, P.-F. (2022) Physcomitrium patens Protoplasting and Protoplast Transfection. In K. Wang and F. Zhang, eds. *Protoplast Technology*. Methods in Molecular Biology. New York, NY: Springer US, pp. 3–19. Available at: https://link.springer.com/10.1007/978-1-0716-2164-6_1 [Accessed September 12, 2022].

Cove, D., Bezanilla, M., Harries, P. and Quatrano, R. (2006) MOSSES AS MODEL SYSTEMS FOR THE STUDY OF METABOLISM AND DEVELOPMENT. *Annu. Rev. Plant Biol.*, **57**, 497–520.

Cove, D.J. and Knight, C.D. (1993) The Moss Physcomitrella patens, a Model System with Potential for the Study of Plant Reproduction. *Plant Cell*, 1483–1488.

Demko, V., Perroud, P.-F., Johansen, W., et al. (2014) Genetic Analysis of *DEFECTIVE KERNEL1* Loop Function in Three-Dimensional Body Patterning in *Physcomitrella patens*. *Plant Physiol.*, **166**, 903–919.

Dominissini, D., Moshitch-Moshkovitz, S., Salmon-Divon, M., Amariglio, N. and Rechavi, G. (2013) Transcriptome-wide mapping of N6-methyladenosine by m6A-seq based on immunocapturing and massively parallel sequencing. *Nat. Protoc.*, **8**, 176–189.

Frank, M.H. and Scanlon, M.J. (2015) Cell-specific transcriptomic analyses of three-dimensional shoot development in the moss Physcomitrella patens. *Plant J. Cell Mol. Biol.*, **83**, 743–751.

Frye, M., Harada, B.T., Behm, M. and He, C. (2018) RNA modifications modulate gene expression during development. *Science*, **361**, 1346.

Garcias Morales, D. and Reyes, J.L. (2021) A birds'-eye view of the activity and specificity of the mRNA m^6A methyltransferase complex. *WIREs RNA*, **12**. Available at: https://onlinelibrary.wiley.com/doi/10.1002/wrna.1618 [Accessed March 24, 2022].

Ge, S.X., Jung, D. and Yao, R. (2020) ShinyGO: a graphical gene-set enrichment tool for animals and plants. *Bioinforma. Oxf. Engl.*, **36**, 2628–2629.

Govindan, G., Sharma, B., Li, Y., Armstrong, C.D., Merum, P., Rohila, J.S., Gregory, B.D. and Sunkar, R. (2022) mRNA N^6-methyladenosine is critical for cold tolerance in Arabidopsis. *Plant J.*, tpj.15872.

Graham, L.E., Cook, M.E. and Busse, J.S. (2000) The origin of plants: Body plan changes contributing to a major evolutionary radiation. *Proc. Natl. Acad. Sci.*, **97**, 4535–4540.

Harrison, C.J., Roeder, A.H.K., Meyerowitz, E.M. and Langdale, J.A. (2009) Local Cues and Asymmetric Cell Divisions Underpin Body Plan Transitions in the Moss Physcomitrella patens. *Curr. Biol.*, **19**, 461–471.

Hu, J., Cai, J., Park, S.J., Lee, K., Li, Y., Chen, Y., Yun, J., Xu, T. and Kang, H. (2021) N^6-Methyladenosine mRNA methylation is important for salt stress tolerance in *Arabidopsis*. *Plant J.*, **106**, 1759–1775.

Ivanova, I., Much, C., Di Giacomo, M., et al. (2017) The RNA m 6 A Reader YTHDF2 Is Essential for the Post-transcriptional Regulation of the Maternal Transcriptome and Oocyte Competence. *Mol. Cell*, **67**, 1059-1067.e4.

Johansen, W., Ako, A.E., Demko, V., Perroud, P.-F., Rensing, S.A., Mekhlif, A.K. and Olsen, O.-A. (2016) The DEK1 calpain Linker functions in three-dimensional body patterning in Physcomitrella patens. *Plant Physiol.*, pp.00925.2016.

Johri, M.M. and Desai, S. (1973) Auxin Regulation of Caulonema Formation in Moss Protonema. *Nature. New Biol.*, **245**, 223–224.

Langmead, B. and Salzberg, S.L. (2012) Fast gapped-read alignment with Bowtie 2. *Nat. Methods*, **9**, 357–359.

Lopez-Obando, M., Hoffmann, B., Géry, C., Guyon-Debast, A., Téoulé, E., Rameau, C., Bonhomme, S. and Nogué, F. (2016) Simple and Efficient Targeting of Multiple Genes Through CRISPR-Cas9 in Physcomitrella patens. *G3 GenesGenomesGenetics*, **6**, 3647–3653.

Luo, G.-Z., MacQueen, A., Zheng, G., et al. (2014) Unique features of the m6A methylome in Arabidopsis thaliana. *Nat. Commun.*, **5**, 5630.

Meinke, D.W. and Sussex, I.M. (1979) Embryo-lethal mutants of Arabidopsis thaliana: a model system for genetic analysis of plant embryo development. *Dev. Biol.*, **72**, 50–61.

Menand, B., Calder, G. and Dolan, L. (2007) Both chloronemal and caulonemal cells expand by tip growth in the moss Physcomitrella patens. *J. Exp. Bot.*, **58**, 1843–1849.

Moody, L.A. (2019) The 2D to 3D growth transition in the moss Physcomitrella patens. *Curr. Opin. Plant Biol.*, **47**, 88–95.

Moody, L.A., Kelly, S., Rabbinowitsch, E. and Langdale, J.A. (2018) Genetic Regulation of the 2D to 3D Growth Transition in the Moss Physcomitrella patens. *Curr. Biol.*, **28**, 473-478.e5.

Niklas, K.J. (2000) The Evolution of Plant Body Plans—A Biomechanical Perspective. *Ann. Bot.*, **85**, 411–438.

Perroud, P., Demko, V., Johansen, W., Wilson, R.C., Olsen, O. and Quatrano, R.S. (2014) Defective Kernel 1 (DEK 1) is required for three-dimensional growth in *P hyscomitrella patens* . *New Phytol.*, **203**, 794–804.

Perroud, P.-F., Meyberg, R., Demko, V., Quatrano, R.S., Olsen, O.-A. and Rensing, S.A. (2020) DEK1 displays a strong subcellular polarity during Physcomitrella patens 3D growth. *New Phytol.*, **226**, 1029–1041.

Robinson, M.D., McCarthy, D.J. and Smyth, G.K. (2010) edgeR: a Bioconductor package for differential expression analysis of digital gene expression data. *Bioinforma. Oxf. Engl.*, **26**, 139–140.

Růžička, K., Zhang, M., Campilho, A., et al. (2017) Identification of factors required for m6A mRNA methylation in Arabidopsis reveals a role for the conserved E3 ubiquitin ligase HAKAI. *New Phytol.*, **215**, 157–172.

Shen, L., Liang, Z., Gu, X., et al. (2016) N 6 -Methyladenosine RNA Modification Regulates Shoot Stem Cell Fate in Arabidopsis. *Dev. Cell*, **38**, 186–200.

Shi, H., Wei, J. and He, C. (2019) Where, When, and How: Context-Dependent Functions of RNA Methylation Writers, Readers, and Erasers. *Mol. Cell*, **74**, 640–650.

Sun, J.G., Yao, X.L., Yang, Z.X. and Zhu, Z.P. (1998) An Arabidopsis embryonic lethal mutant with reduced expression of alanyl-tRNA synthetase gene. *Cell Res.*, **8**, 119–134.

Wang, Y.-J., Yang, B., Lai, Q., et al. (2021) Reprogramming of m6A epitranscriptome is crucial for shaping of transcriptome and proteome in response to hypoxia. *RNA Biol.*, **18**, 131–143.

Wickett, N.J., Mirarab, S., Nguyen, N., et al. (2014) Phylotranscriptomic analysis of the origin and early diversification of land plants. *Proc. Natl. Acad. Sci.*, **111**, E4859–E4868.

Xu, Z., Shi, X., Bao, M., et al. (2021) Transcriptome-Wide Analysis of RNA m6A Methylation and Gene Expression Changes Among Two Arabidopsis Ecotypes and Their Reciprocal Hybrids. *Front. Plant Sci.*, **12**. Available at: https://www.frontiersin.org/article/10.3389/fpls.2021.685189 [Accessed June 7, 2022].

Yue, H., Nie, X., Yan, Z. and Weining, S. (2019) N6-methyladenosine regulatory machinery in plants: composition, function and evolution. *Plant Biotechnol. J.*, **17**, 1194–1208.

Zhang, Y., Liu, T., Meyer, C.A., et al. (2008) Model-based analysis of ChIP-Seq (MACS). *Genome Biol.*, **9**, R137.

Zhong, S., Li, H., Bodi, Z., Button, J., Vespa, L., Herzog, M. and Fray, R.G. (2008) MTA Is an Arabidopsis Messenger RNA Adenosine Methylase and Interacts with a Homolog of a Sex-Specific Splicing Factor. *Plant Cell*, **20**, 1278–1288.

Zhou, L., Gao, G., Tang, R., Wang, W., Wang, Y., Tian, S. and Qin, G. (2022) m ^{6} A-mediated regulation of crop development and stress responses. *Plant Biotechnol. J.*, pbi.13792.

(a)

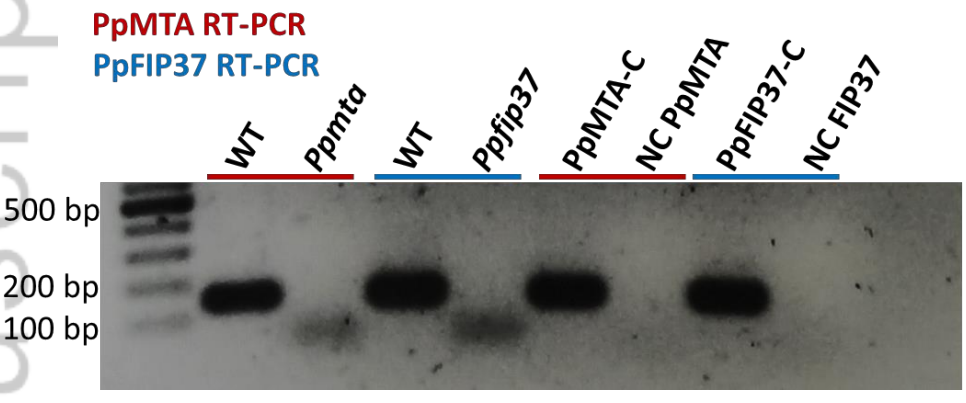

(b)

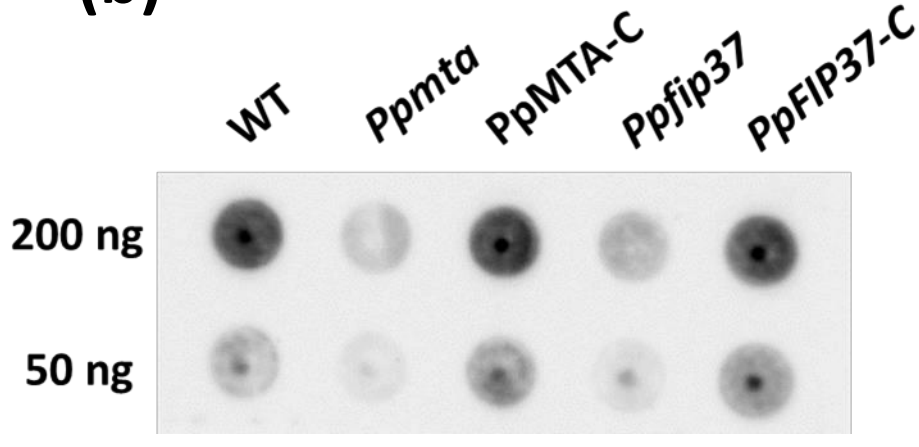

(c)

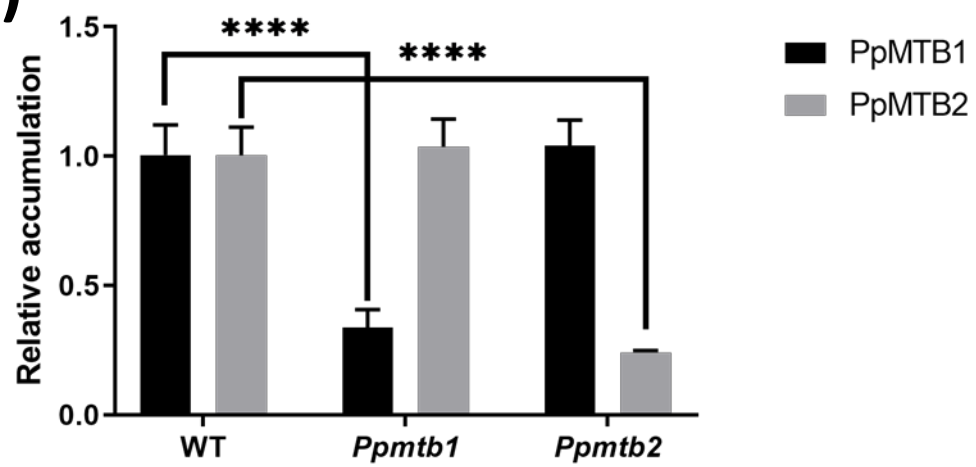

(d)

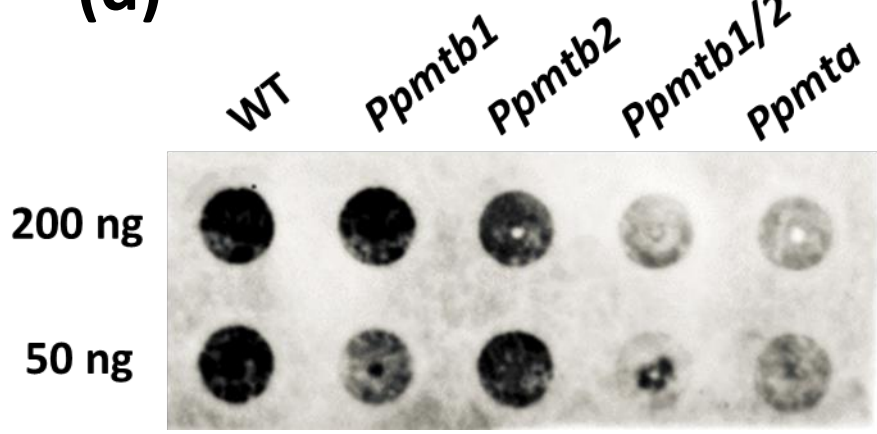

(a)

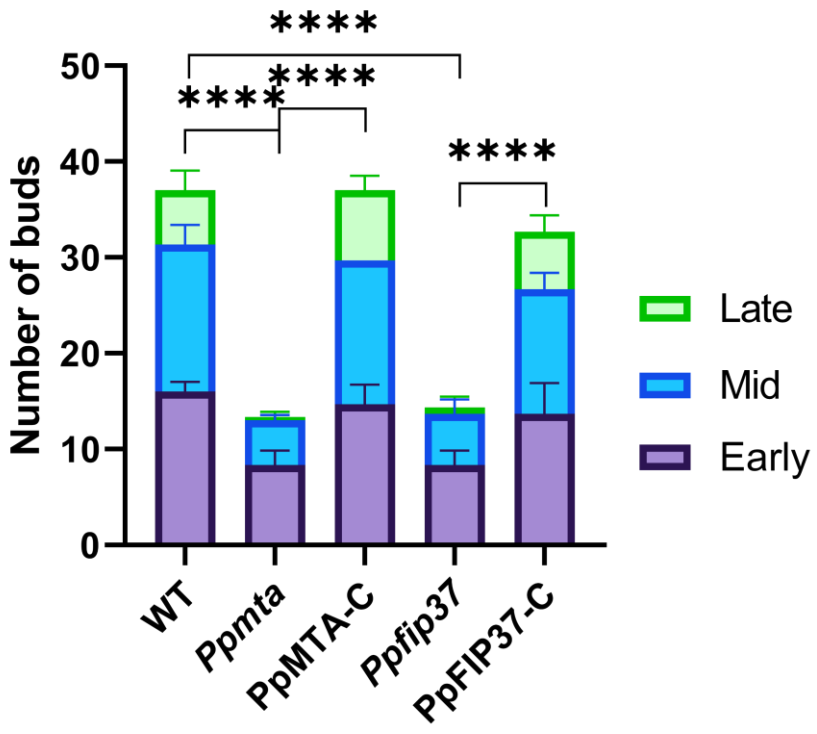

(b)

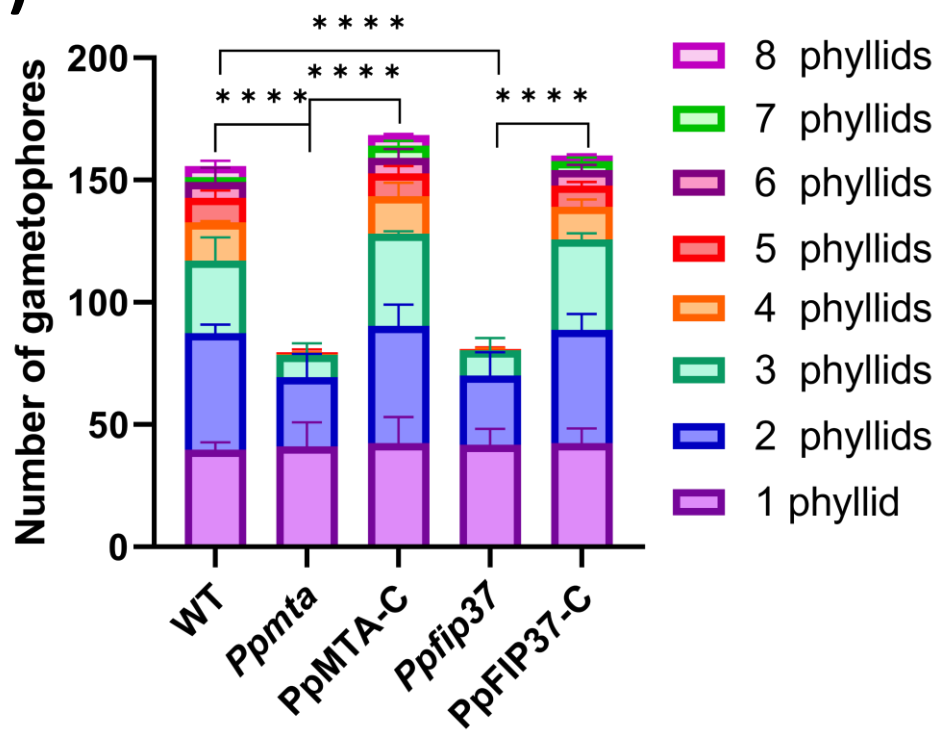

(c)

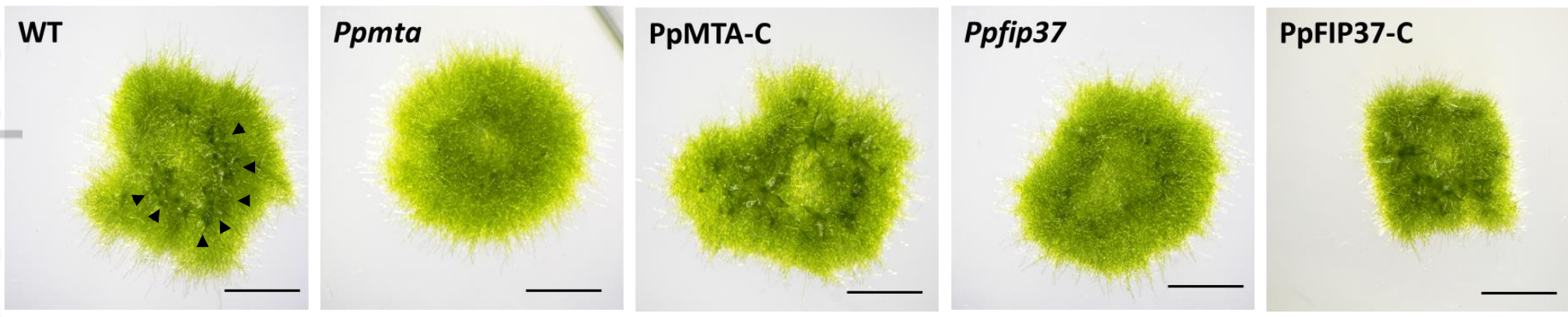

(d)

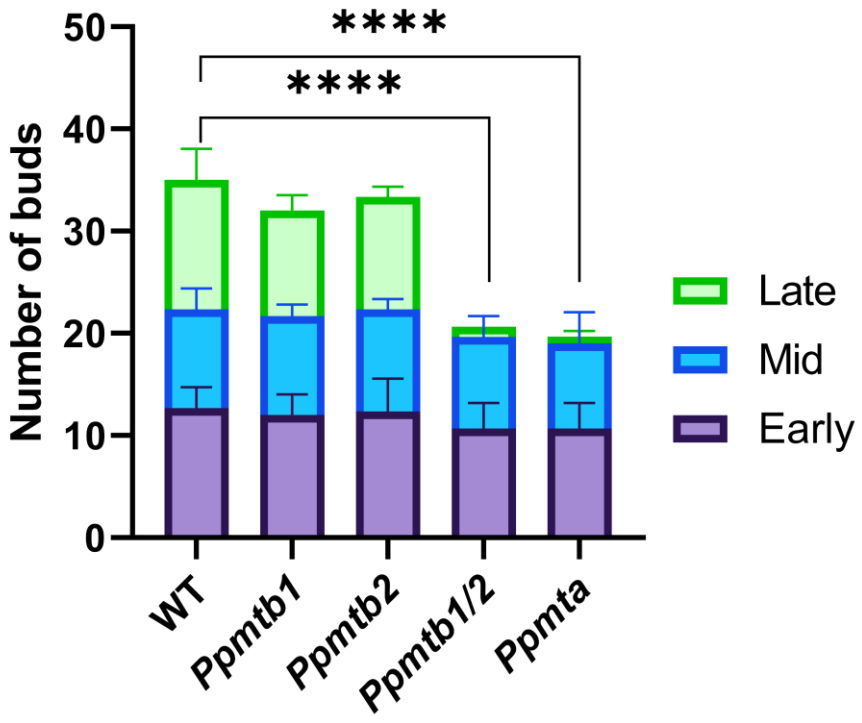

(e)

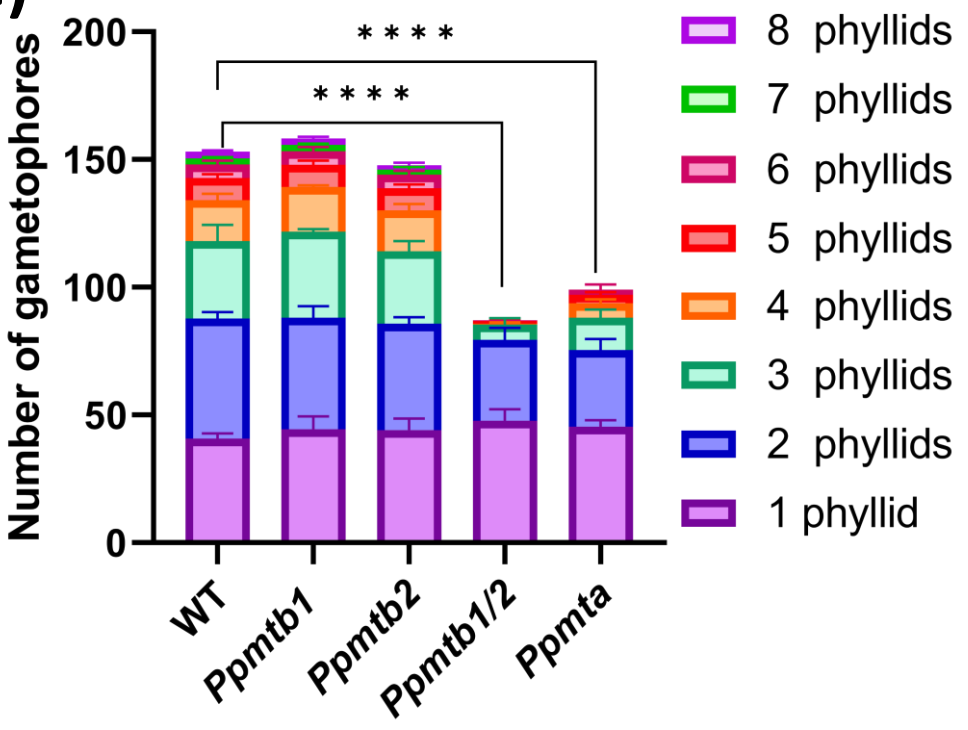

(f)

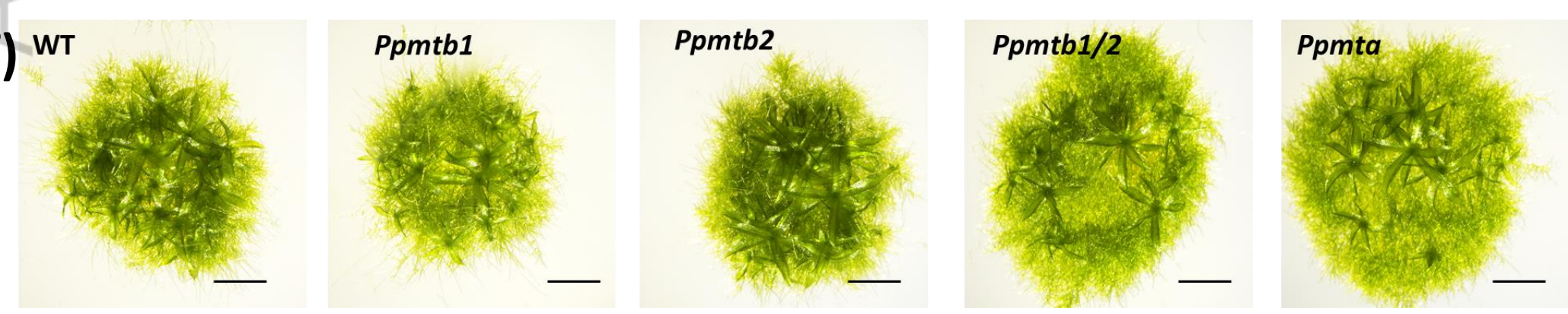

(a)

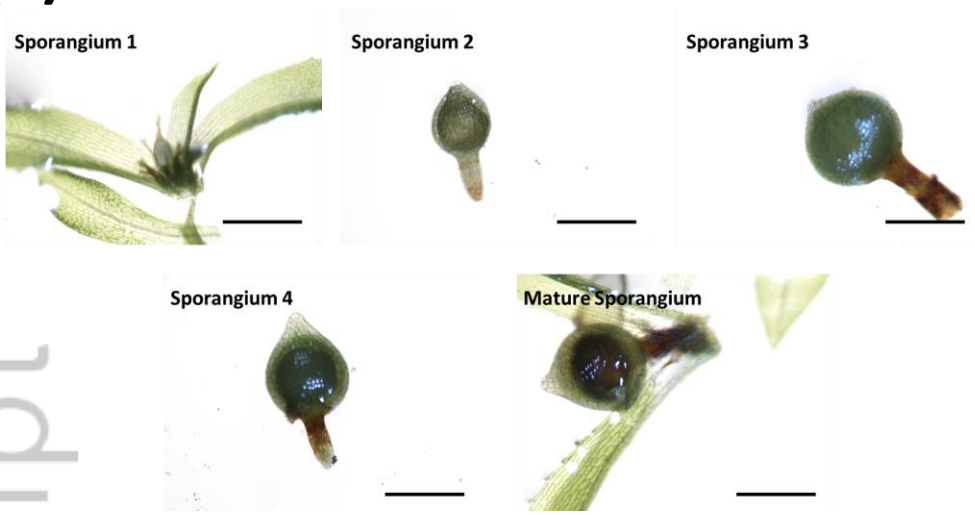

(b)

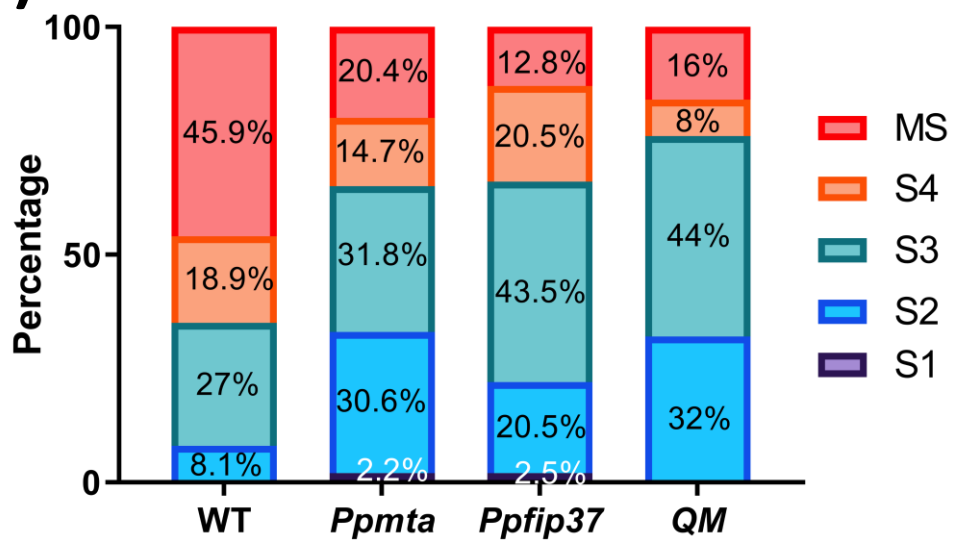

(c)

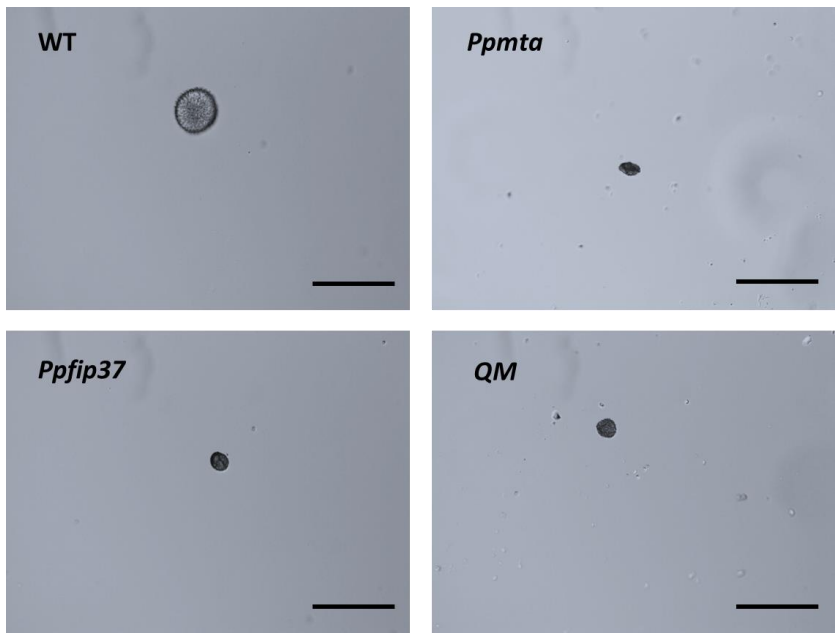

(d)

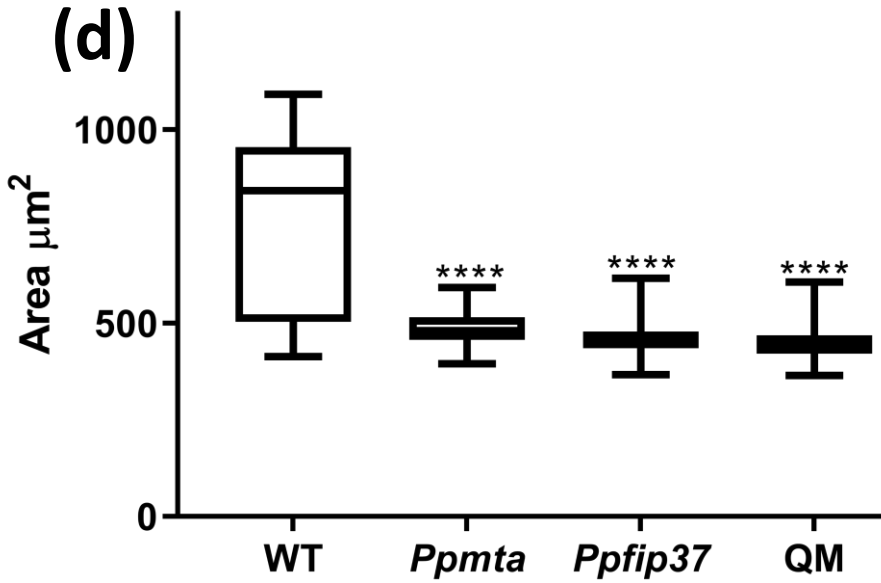

(e)

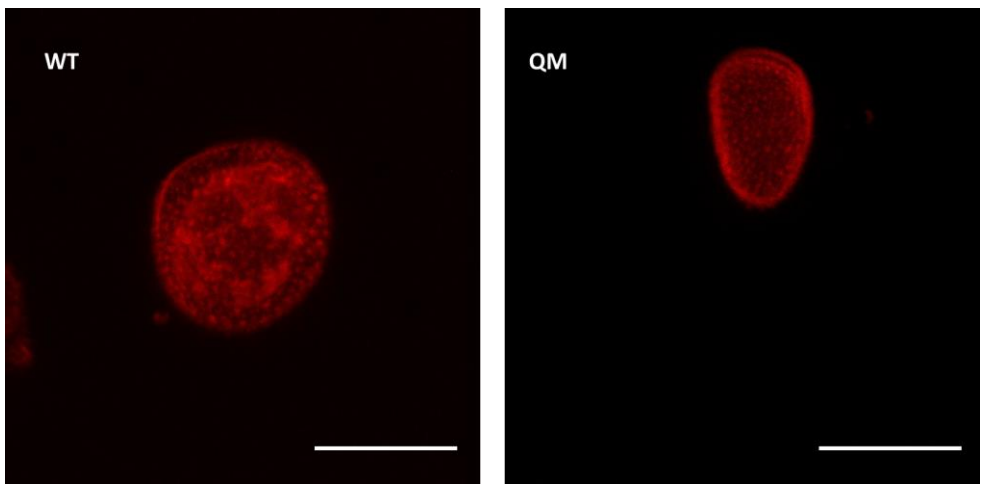

(f)

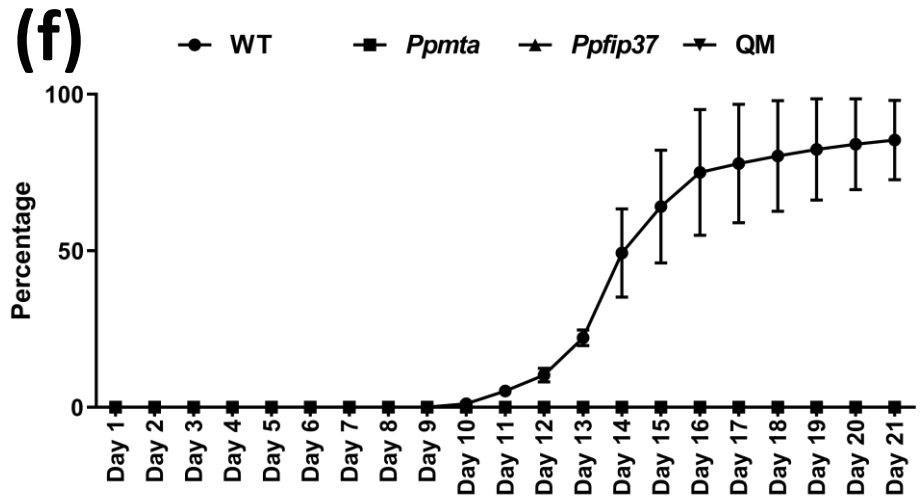

(a)

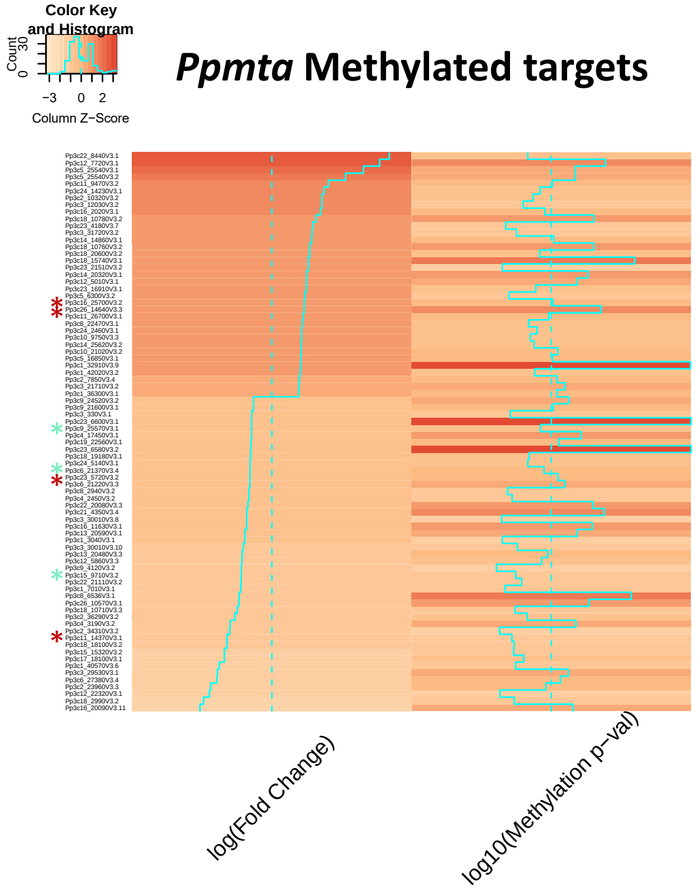

(b)

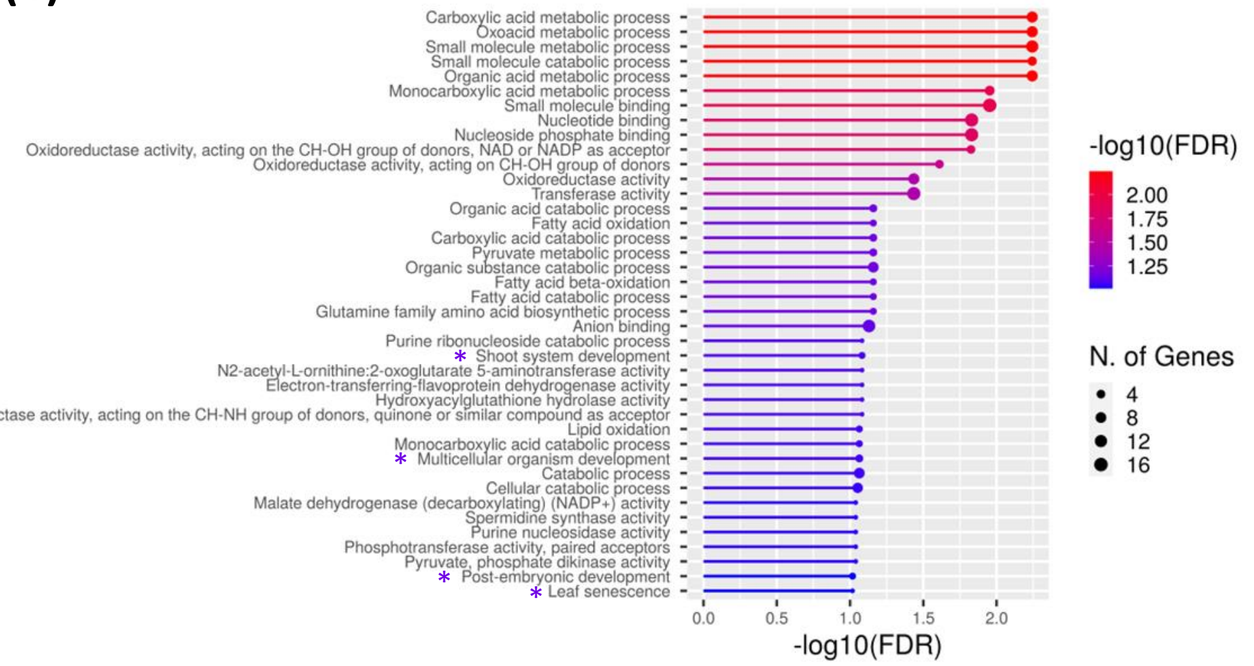

(c)

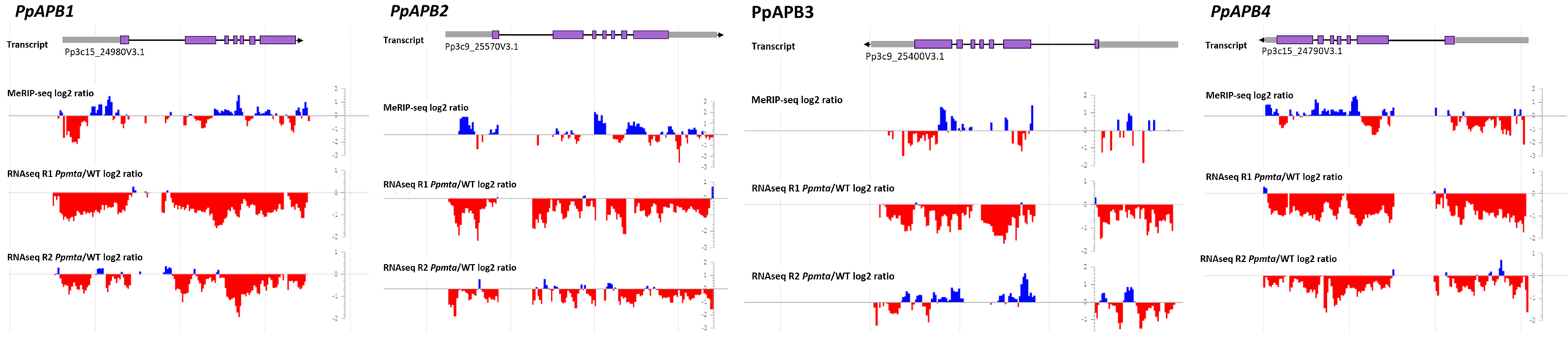

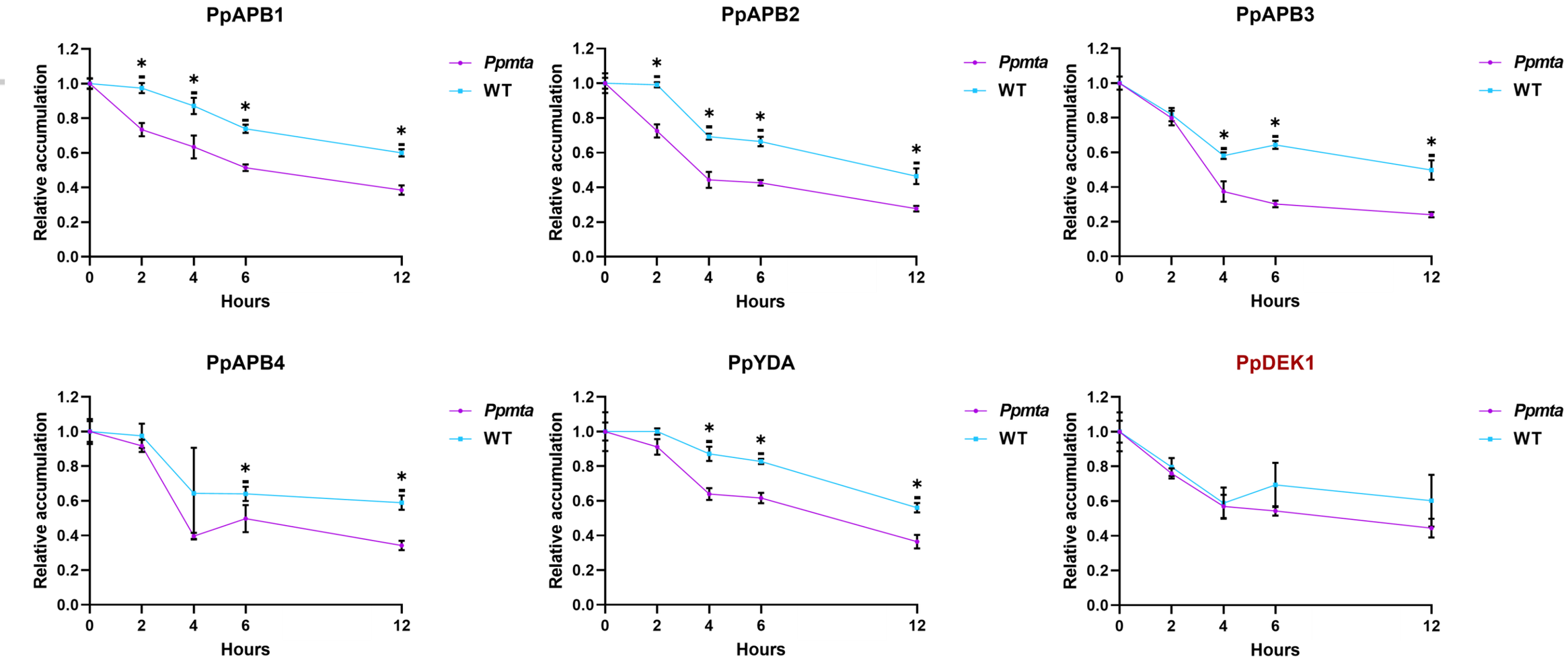

actinomycin D / mock treatment (h)

(a)

PpACT

MP Input no-m^{6}A m^{6}A NG

300 bp
200 bp
100 bp

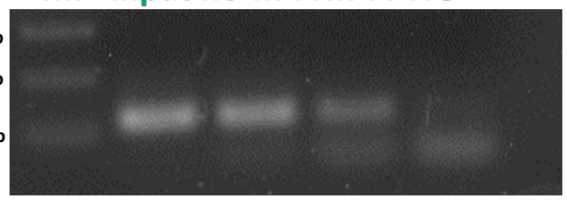

PpDEK1

MP Input no-m^{6}A m^{6}A NG

300 bp
200 bp
100 bp

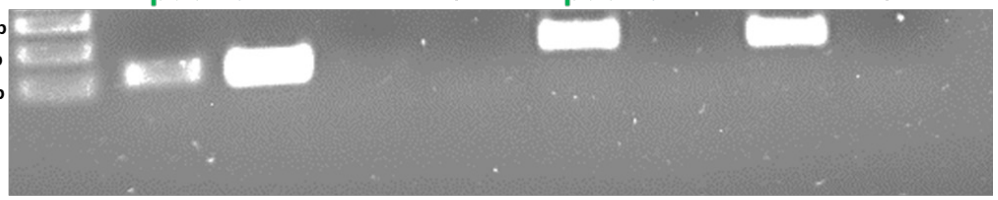

PpYDA

Input no-m^{6}A m^{6}A NG

PpUBI10

MP Input no-m^{6}A m^{6}A NG

300 bp
200 bp
100 bp

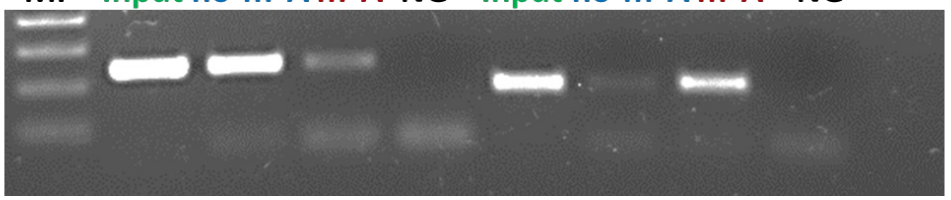

PpAPB1

Input no-m^{6}A m^{6}A NG

(b)

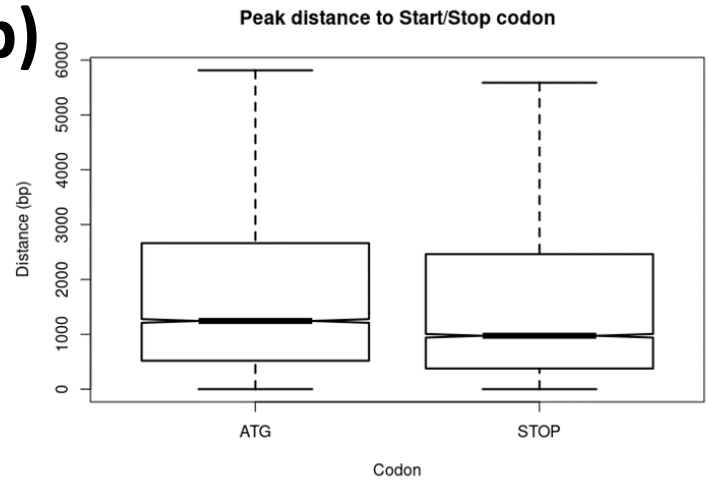

(c)

(d)

PpAPB1

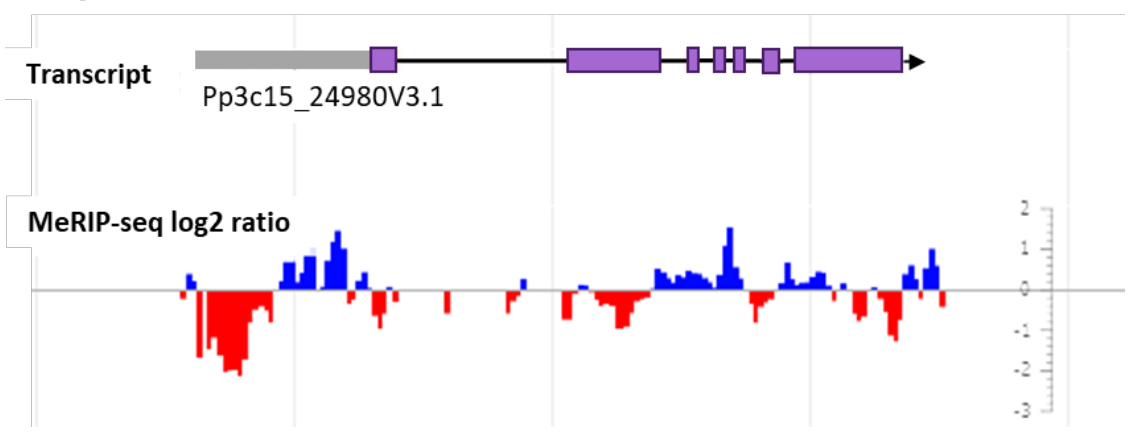

PpAPB2

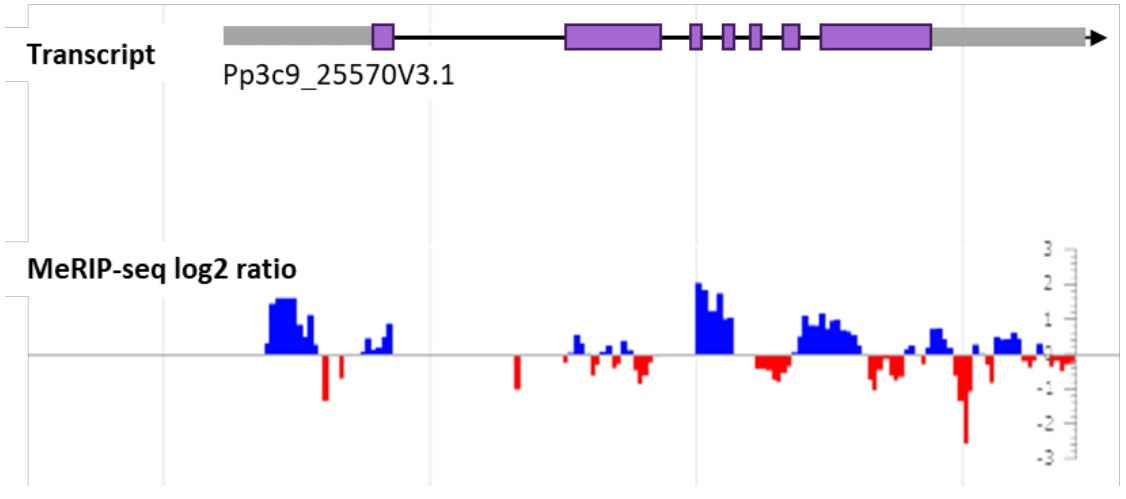

(e)

PpAPB2

M Input m^{6}A no-m^{6}A NG

300 bp
200 bp
100 bp

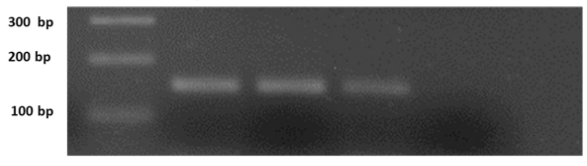

PpAPB3

M Input m^{6}A no-m^{6}A NG

300 bp
200 bp
100 bp

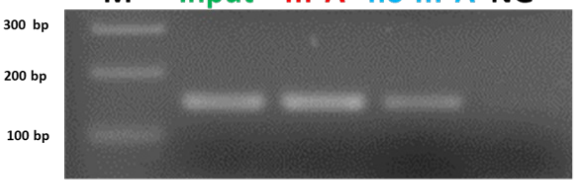

PpAPB4

M Input m^{6}A no-m^{6}A NG

300 bp
200 bp
100 bp

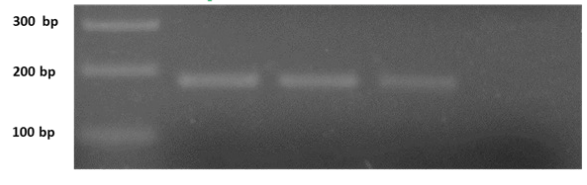

PpACT

M Input m^{6}A no-m^{6}A NG

300 bp
200 bp
100 bp